Necl2/3-mediated mechanism for tripartite synapse formation

Nozawa, Osamu ; Miyata, Muneaki ; Shiotani, Hajime ; Kameyama, Takeshi ; Komaki, Ryouhei ; Shimizu, Tatsuhiro ; Kuriu, Toshihiko ; Kashiwagi,…

(Citation)
Development,150(4):dev200931

(Issue Date)
2023-02-22

(Resource Type)
journal article

(Version)
Version of Record

© 2023. Published by The Company of Biologists Ltd | Development (2023) 150, dev200931. doi:10.1242/dev.200931

RESEARCH ARTICLE

Necl2/3-mediated mechanism for tripartite synapse formation

Osamu Nozawa[1,*], Muneaki Miyata[1,*], Hajime Shiotani[1], Takeshi Kameyama[1], Ryouhei Komaki[1], Tatsuhiro Shimizu[1], Toshihiko Kuriu[2], Yutaro Kashiwagi[3], Yuka Sato[3], Michinori Koebisu[4], Atsu Aiba[4], Shigeo Okabe[3], Kiyohito Mizutani[1,‡] and Yoshimi Takai[1,‡]

ABSTRACT

Ramified, polarized protoplasmic astrocytes interact with synapses via perisynaptic astrocyte processes (PAPs) to form tripartite synapses. These astrocyte-synapse interactions mutually regulate their structures and functions. However, molecular mechanisms for tripartite synapse formation remain elusive. We developed an *in vitro* co-culture system for mouse astrocytes and neurons that induced astrocyte ramifications and PAP formation. Co-cultured neurons were required for astrocyte ramifications in a neuronal activity-dependent manner, and synaptically-released glutamate and activation of astrocytic mGluR5 metabotropic glutamate receptor were likely involved in astrocyte ramifications. Astrocytic Necl2 *trans*-interacted with axonal Necl3, inducing astrocyte-synapse interactions and astrocyte functional polarization by recruiting EAAT1/2 glutamate transporters and Kir4.1 K^+ channel to the PAPs, without affecting astrocyte ramifications. This Necl2/3 *trans*-interaction increased functional synapse number. Thus, astrocytic Necl2, synaptically-released glutamate and axonal Necl3 cooperatively formed tripartite glutamatergic synapses *in vitro*. Studies on hippocampal mossy fiber synapses in *Necl3* knockout and *Necl2/3* double knockout mice confirmed these previously unreported mechanisms for astrocyte-synapse interactions and astrocyte functional polarization *in vivo*.

KEY WORDS: Tripartite synapse, Astrocyte, Neuron, Cell adhesion molecule, Necl, Glutamate transporter

INTRODUCTION

Synapses connect individual neurons to form an information-processing neuronal network that is crucial for learning and memory (Takeuchi et al., 2014). Synapses interact with intricate terminal processes of highly ramified and polarized astrocytes, called perisynaptic astrocyte processes (PAPs). Presynaptic and postsynaptic components, together with the PAPs, form functional units, known as tripartite synapses (Araque et al., 1999; Haydon, 2001; Mauch et al., 2001). Astrocytes secrete various synaptogenic molecules, such as apolipoprotein E3 (ApoE3), cholesterol, thrombospondin, secreted protein acidic and cysteine rich (SPARC), hevin, glypican, transforming growth factor β (TGF-β) and chordin-like 1 (Allen et al., 2012; Blanco-Suarez et al., 2018; Christopherson et al., 2005; Diniz et al., 2012; Jones et al., 2011; Kucukdereli et al., 2011; Perea et al., 2009; Sun et al., 1998). In turn, astrocyte morphology is regulated by factors, such as fibroblast growth factor 2 (FGF2), BMP2/4, LIF and TGF-β, some of which may be secreted from neurons (Bonaguidi et al., 2005; Reilly et al., 1998). Direct cell-cell interactions are thought to be involved in astrocyte-synapse interactions. Previously reported cell adhesion molecules (CAMs) include NCAM, Ng-CAM, ephrin A3, Necl2 (SynCAM1; CADM1), protocadherin-γC5, neuroligin 1/2/3 and neurexins (Garrett and Weiner, 2009; Li et al., 2010; Pannasch et al., 2014; Stogsdill et al., 2017; Takano et al., 2020). Astrocyte-synapse interactions are involved not only in learning and memory, but also in age-related dysfunction and degeneration of synapses, leading to the decline of cognitive functions (Blanco-Suárez et al., 2017). Furthermore, astrocytes are believed to be crucial in synaptic degeneration and neuronal death caused by neuropathological conditions, such as Alzheimer's disease, Parkinson's disease, epilepsy and stroke (Blanco-Suárez et al., 2017).

The PAPs are enriched with EAAT1 (GLAST; SLC1A3) and EAAT2 (GLT1; SLC1A2) glutamate transporters and Kir4.1 (KCNJ10) inward rectifier K^+ channel, which are essential molecular components in astrocyte functional polarization (Danbolt et al., 1992; Lehre et al., 1995; Nagelhus et al., 2004). EAAT1/2 and Kir4.1 take up excess extracellular glutamate and K^+ released from glutamatergic presynaptic terminals (Danbolt et al., 2016; Djukic et al., 2007). Excess extracellular glutamate leads to neuronal cell death through supranormal activation of glutamate receptors, known as excitotoxicity (Danbolt, 2001). Furthermore, an aberrant increase in extracellular K^+ is associated with epilepsy (Nwaobi et al., 2014, 2016). Therefore, precisely controlled placement and functions of the PAPs in tripartite synapses may crucially affect the vulnerability of neurons and neuronal networks. However, molecular mechanisms for astrocyte ramifications, astrocyte-synapse interactions and astrocyte functional polarization during tripartite synapse formation have not been fully understood. In addition, mechanisms for synapse degeneration associated with astrocytic dysfunction in aging and diseases are largely unknown.

To better understand molecular mechanisms supporting these processes, it is helpful to develop co-culture systems for astrocytes and neurons that replicate tripartite synapse formation *in vivo*, but the technical hurdles to obtain fully differentiated astrocytes *in vitro* have been challenging to overcome. Recently, Stogsdill et al. developed an *in vitro* co-culture system for rat cortical astrocytes and neurons (Stogsdill et al., 2017), which showed that neuregulins and neurexins are involved in astrocyte-synapse interactions. However, the astrocytes in their co-culture system did not fully ramify to form many numerous fine terminals as observed *in vivo*, and the functions of these cell adhesion molecules in recruiting

[1]Division of Pathogenetic Signaling, Department of Physiology and Cell Biology, Kobe University Graduate School of Medicine, Kobe, Hyogo 650-0047, Japan. [2]Osaka Medical and Pharmaceutical University, Research and Development Center, Takatsuki, Osaka 569-8686, Japan. [3]Department of Cellular Neurobiology, Graduate School of Medicine, The University of Tokyo, Tokyo 113-0033, Japan. [4]Section of Animal Research and Laboratory of Animal Resources, Center for Disease Biology and Integrative Medicine, Graduate School of Medicine, The University of Tokyo, Tokyo 113-0033, Japan.
*These authors contributed equally to this work

‡Authors for correspondence (ytakai@med.kobe-u.ac.jp; mizutani@med.kobe-u.ac.jp)

M.K., 0000-0002-6451-3409; K.M., 0000-0003-1758-8026; Y.T., 0000-0003-1338-1327

Handling Editor: François Guillemot
Received 16 May 2022; Accepted 23 November 2022

Development (2023) 150, dev200931. doi:10.1242/dev.200931

EAAT1/2 and Kir4.1 to the PAPs for astrocyte functional polarization remained unknown. Here, we developed a novel *in vitro* co-culture system for mouse ganglionic eminence astrocytes and mouse hippocampal neurons that induced astrocyte ramifications, astrocyte-synapse interactions and astrocyte functional polarization, forming tripartite synapses morphologically and functionally similar to those *in vivo*. Using this system, we discovered mechanisms supporting major astrocyte functions.

RESULTS

Co-cultured neurons are required for astrocyte ramifications in a neuronal activity-dependent manner

We first prepared mouse ganglionic eminence astrocytes expressing membrane anchored GAP43 fragment fused to GFP (GFP-Mem-astrocytes) to visualize the intricate structure of terminal processes (Moriyoshi et al., 1996). Without neurons, GFP-Mem-astrocytes frequently showed round and flat shapes with no fine terminal processes (Fig. 1A), or they took polygonal shapes with several thick processes, as described previously (Bambrick et al., 1996; Booher and Sensenbrenner, 1972; Chojnacki and Weiss, 2008). However, astrocytes co-cultured with neurons formed radially oriented and highly ramified processes that gradually branched into finer terminal processes, ending near VGLUT1 (SLC17A7) signal-positive glutamatergic synapses (Fig. 1B, see Fig. 2A), although the extent of ramifications varied depending on co-culture conditions (Fig. S1A). Of the VGLUT1 signal, 91.8±4.5% (mean±s.e.m.) colocalized with the postsynaptic density (PSD) protein PSD95 (DLG4) signal (Cho et al., 1992) and 90.2±3.4% with neurabin II (spinophilin; PPP1R9b) signal (Allen et al., 1997; Nakanishi et al., 1997; Satoh et al., 1998), indicating that the VGLUT1 signal is a reliable synaptic marker in our newly developed co-culture system (Fig. 1C). Neurons functionally inactivated with methanol did not induce astrocyte ramifications with numerous fine terminal processes (hereafter referred to as 'ramifications') (Fig. S2A). Time-lapse imaging revealed that undifferentiated GFP-Mem-astrocytes were motile and showed round morphology with a few short processes (Movie 1). This highly branched astrocytic morphology was established through repetitive extension and retraction of individual branches and their progressive stabilization (Movies 1 and 2). Some of the thin terminal branches contacted neuronal processes, resulting in either process retraction or further extension using neuronal processes as guides. The latter events seemingly facilitate astrocytic processes reaching synaptic sites. These results indicate that co-cultured neurons induce branching of astrocytic processes through dynamic cell-cell interactions.

Astrocyte ramifications induced by co-cultured neurons were blocked by the sodium channel blocker tetrodotoxin (TTX), although some fine terminal processes continued to move (Fig. 1D,E; Movie 3). Application of glutamate to the TTX-pretreated culture did not restore branching activity of astrocytes (Fig. 1D,E). Furthermore, TTX treatment was ineffective at eliminating already-established branched processes of mature GFP-Mem-astrocytes (Fig. S2B; Movie 4). Glutamate did not induce ramifications of GFP-Mem-astrocytes cultured without neurons (Fig. S2C,D). Extensive ramifications of GFP-Mem-astrocytes induced by co-cultured neurons were inhibited by the mGluR3/5 antagonist MCPG and the mGluR5 antagonist MPEP (Fig. 1F,G), but not by the mGluR3 antagonist LY395756, the AMPA receptor antagonist CNQX or the NMDA receptor antagonist D-AP5 (Fig. S2E,F). These results indicate that co-cultured neurons are required for astrocyte ramifications in a neuronal activity-dependent manner and suggest that at least synaptically-released glutamate and astrocytic mGluR5 are involved in astrocyte ramifications, although the possible involvement of other neurotransmitters and neuronal mGluR5 in astrocyte ramifications could not be completely excluded.

Astrocytic Necl2 and axonal Necl3 are involved in astrocyte-synapse interactions and astrocyte functional polarization *in vitro*

If the ramified morphology of astrocytes reflects their functional maturation, molecules essential for astrocytic regulation of synapses may be recruited to the PAPs. To test this possibility, we first analyzed the localization of EAAT2, the predominant glutamate transporter in the PAPs *in vivo* (Lehre et al., 1995). The EAAT2 signal localized near VGLUT1 signal-positive synapses in GFP-Mem-astrocytes co-cultured with neurons (Fig. 2A-1-A-3,C, see Fig. 4A), indicating that the PAPs of ramified astrocytes co-cultured with neurons recruited the molecular component essential for the uptake of synaptically-released glutamate. The EAAT2 signal that did not colocalize with the GFP-Mem signal was observed (Fig. 2A-1), but this signal was derived from astrocytes into which GFP-Mem was not introduced, because the transfection efficiency of GFP-Mem into astrocytes was ∼30%.

We previously demonstrated crucial roles of the nectin and Necl family members in the localization and functions of other membrane receptors and integrins via their *cis*-interactions (Takai et al., 2008a,b). Immunolocalization of the nectin and Necl family proteins in the mouse hippocampal CA3 region (CA3) supports their possible involvement in synaptogenesis, especially nectin 1/3 localized at puncta adherentia junctions (PAJs) of hippocampal mossy fiber tripartite synapses (Mizoguchi et al., 2002). Strong enrichment of the Necl2 and Necl3 (CADM2) signals, together with weak accumulation of the Necl1 (CADM3) and Necl4 (CADM4) signals, was observed at the CA3 stratum lucidum where mossy fiber tripartite synapses are located, and the Necl2/3 signals localized near the EAAT2 signal (see Fig. 7A,B). Screening of Necl immunoreactivity in our culture preparation revealed astrocytic expression of Necl1/2/4, a negligible level of astrocytic Necl3 and neuronal expression of all Necl family proteins (Fig. 3A).

The Necl2/3 signals colocalized with the EAAT2 signal in astrocytes co-cultured with neurons near VGLUT1 signal-positive synapses (Fig. 2A-1-A-3,C, see Fig. 4A), consistent with the *in vivo* localization of the Necl2/3 signals near the EAAT2 signal (see Fig. 7B). More than 70% of astrocytic processes reached VGLUT1 signal-positive synapses and colocalized with the Necl2/3 and EAAT2 signals. This EAAT2 signal accumulation in astrocytic fine terminal processes near VGLUT1 signal-positive synapses was reduced but faintly remained in the co-culture of *Necl2*-knockout (KO) astrocytes expressing GFP-Mem (*Necl2*-KO GFP-Mem-astrocytes) with wild-type (WT) neurons (Fig. S3A-1-A-3; see Fig. 4B). The *Necl2*-KO astrocytes were prepared from the systemic *Necl2*-KO mice (Fig. S4A,B). In this condition, the Necl3 signal accumulation near VGLUT1 signal-positive synapses was not significantly reduced (Fig. S3A-3, see Fig. S8). The Necl2 signal still accumulated at VGLUT1 signal-positive puncta (Fig. S3A-1-A-3; see Fig. 4B), but it was derived from co-cultured neurons, because the Necl2 signal disappeared in the co-culture of *Necl2*-KO GFP-Mem-astrocytes with *Necl2*-KO neurons, although the faint background signal remained (Fig. S5). Conversely, the EAAT2 and Necl3 signals near VGLUT1 signal-positive synapses, where the exogenous GFP-Necl2 signal colocalized, increased when astrocytes exogenously expressing GFP-Necl2 (GFP-Necl2-astrocytes) were co-cultured with WT neurons (Fig. 3B-1-B-2,

Development (2023) 150, dev200931. doi:10.1242/dev.200931

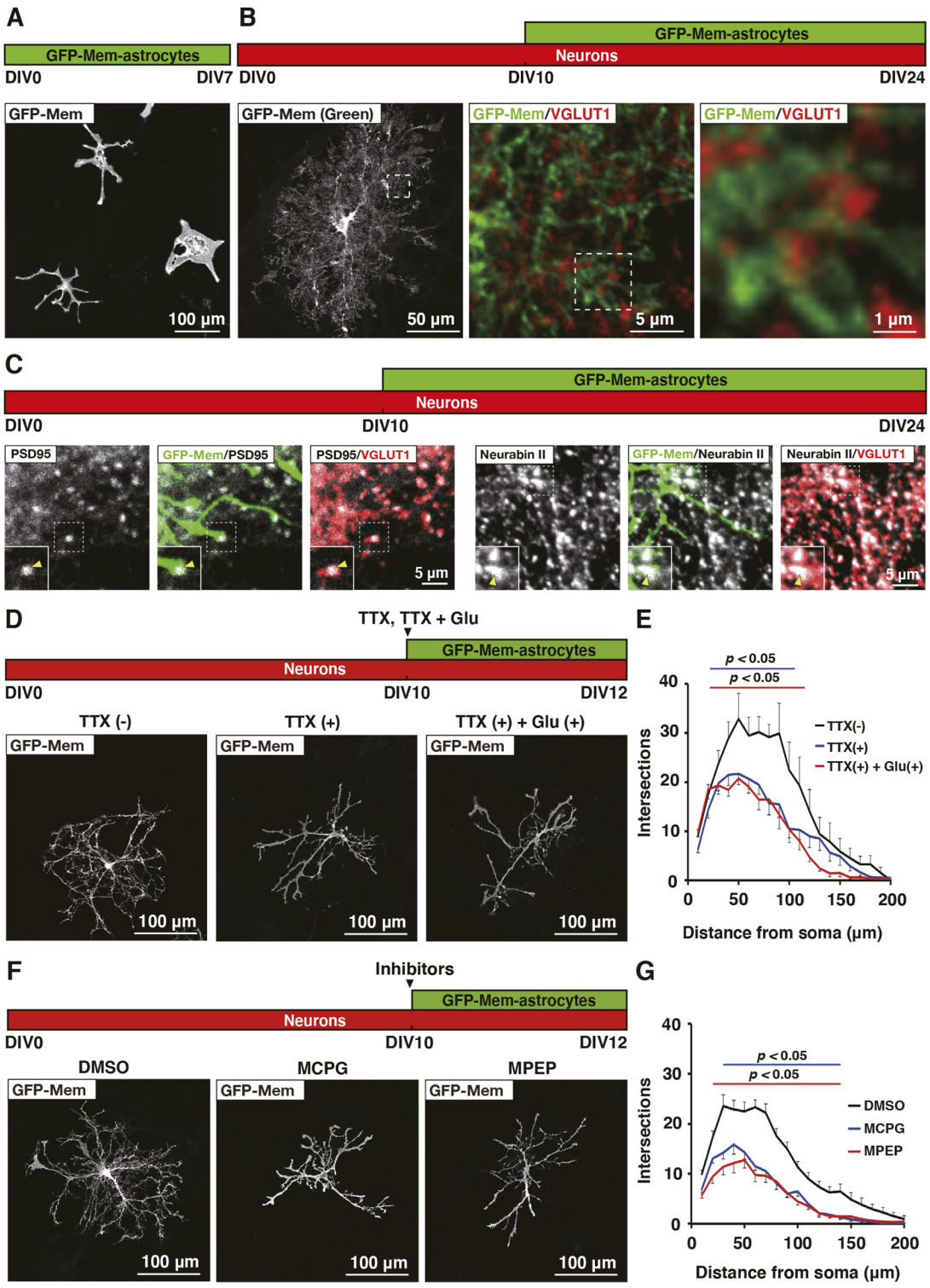

Fig. 1. Astrocyte ramifications induced by co-cultured neurons. Representative IF images using the antibodies indicated in respective panels. (A) Astrocytes cultured without neurons for 7 days. Astrocytes could not be maintained more than 7 days; thus, analysis of neuron-free astrocytes to ≤7 days after plating was limited. (B) Neurons precultured for 10 days, followed by co-culture with GFP-Mem-astrocytes for an additional 14 days. Left panel shows an image using the anti-GFP monoclonal antibody; center panel shows a high magnification image of the boxed region of the left panel using both anti-GFP and anti-VGLUT1 antibodies; and right panel shows a high magnification image of the boxed region of the center panel using both anti-GFP and anti-VGLUT1 antibodies. (C) Colocalization of the VGLUT1 signal with the PSD95 and neurabin II signals. Neurons precultured for 10 days, followed by co-culture with GFP-Mem-astrocytes for an additional 14 days. Yellow arrowheads indicate the PAPs with the VGLUT1, PSD95 or neurabin II signal. Boxed regions are magnified in insets. (D) Neurons precultured for 10 days, followed by co-culture with GFP-Mem-astrocytes for an additional 2 days in the absence or presence of TTX or TTX plus glutamate (Glu). (E) Sholl analysis of astrocyte ramifications in D. (F) Morphology of GFP-Mem-astrocytes in the absence or presence of MCPG or MPEP co-cultured for 2 days with neurons that had been precultured for 10 days. (G) Sholl analysis of astrocyte ramifications in F. Data were compared using two-way ANOVA with the Bonferroni post-hoc test. Data are mean±s.e.m. Images are representative of three independent experiments.

Development (2023) 150, dev200931. doi:10.1242/dev.200931

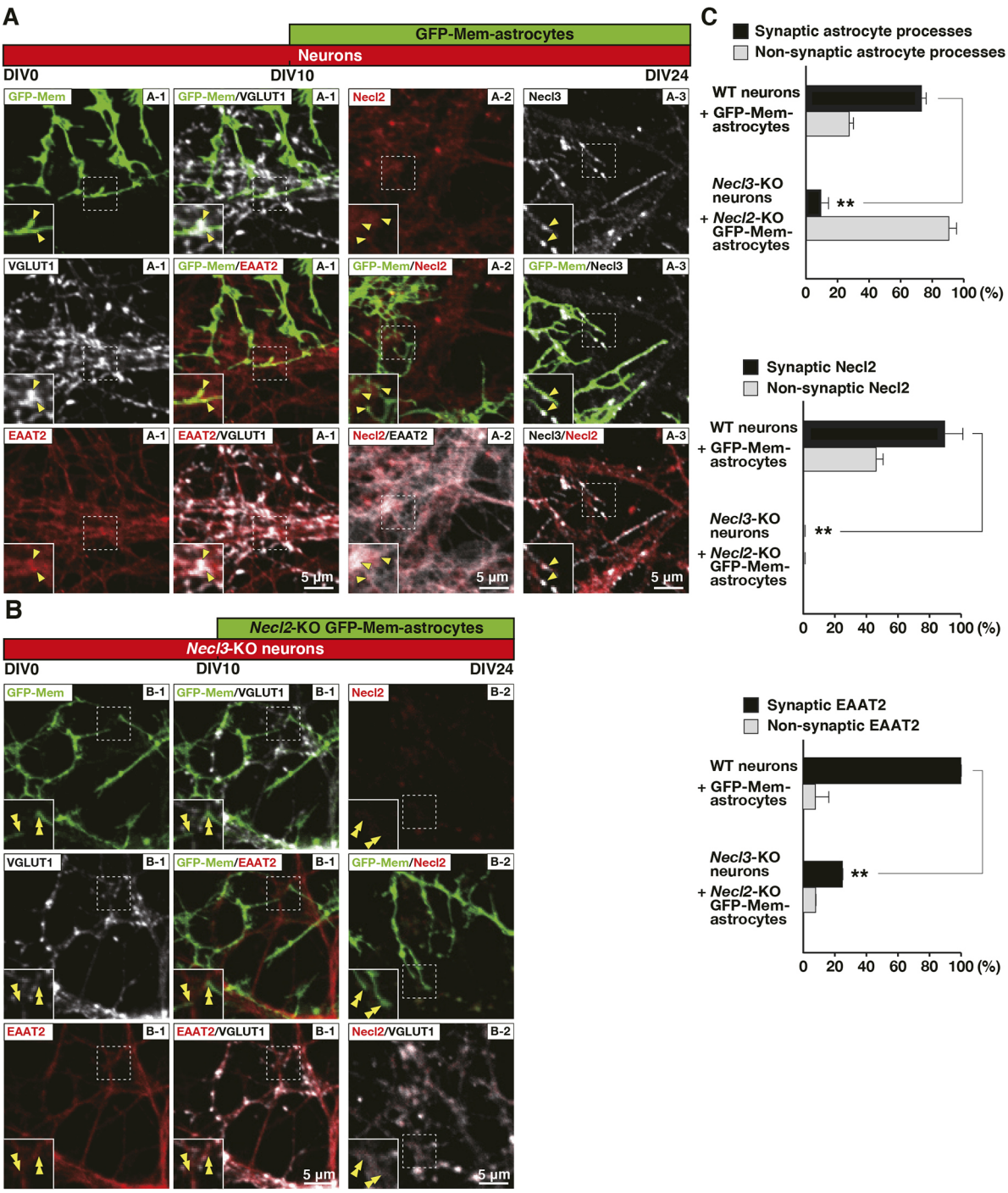

Fig. 2. Astrocytic Necl2- and axonal Necl3-dependent localization of EAAT2 at the PAPs *in vitro*. Representative IF images using the antibodies indicated in respective panels. WT or *Necl3*-KO neurons precultured for 10 days, followed by co-culture with GFP-Mem- or *Necl2*-KO GFP-Mem-astrocytes for an additional 14 days. Boxed regions are magnified in insets. (A) WT neurons and GFP-Mem-astrocytes. Yellow arrowheads indicate the PAPs with the VGLUT1, EAAT2, Necl2 or Necl3 signal. The Necl2/3 signals colocalized with the EAAT2 signal near VGLUT1 signal-positive synapses. The labels A-1, A-2 and A-3 each refer to images in the same field. (B) *Necl3*-KO neurons and *Necl2*-KO GFP-Mem-astrocytes. Yellow double arrowheads indicate the PAPs without the EAAT2 or VGLUT1 signal. The EAAT2 signal was diminished near VGLUT1 signal-positive synapses. The labels B-1 and B-2 each refer to images in the same field. (C) Quantification of the astrocytic terminal processes that reached VGLUT1 signal-positive synapses and of the localization of the Necl2 and EAAT2 signal-positive puncta in A and B. The astrocytic terminal processes that reached VGLUT1 signal-positive synapses were defined as 'synaptic astrocyte processes' and those that did not were defined as 'non-synaptic astrocyte processes'. Data are mean±s.e.m. $^{**}P<0.01$ (one-way ANOVA, followed by Tukey-Kramer honestly significant difference post-hoc test). NS, not significant. Images are representative of three independent experiments.

see Fig. 4C). Thus, manipulation of astrocytic Necl2 *in vitro* indicated an essential role of astrocytic Necl2 in recruitment of EAAT2 to the PAPs. We next evaluated the function of neuronal Necl3 in tripartite synapse formation. *Necl3*-KO neurons did not induce proper placement of the EAAT2, Necl2 and GFP-Necl2 signal-positive puncta near VGLUT1 signal-positive synapses in

Development (2023) 150, dev200931. doi:10.1242/dev.200931

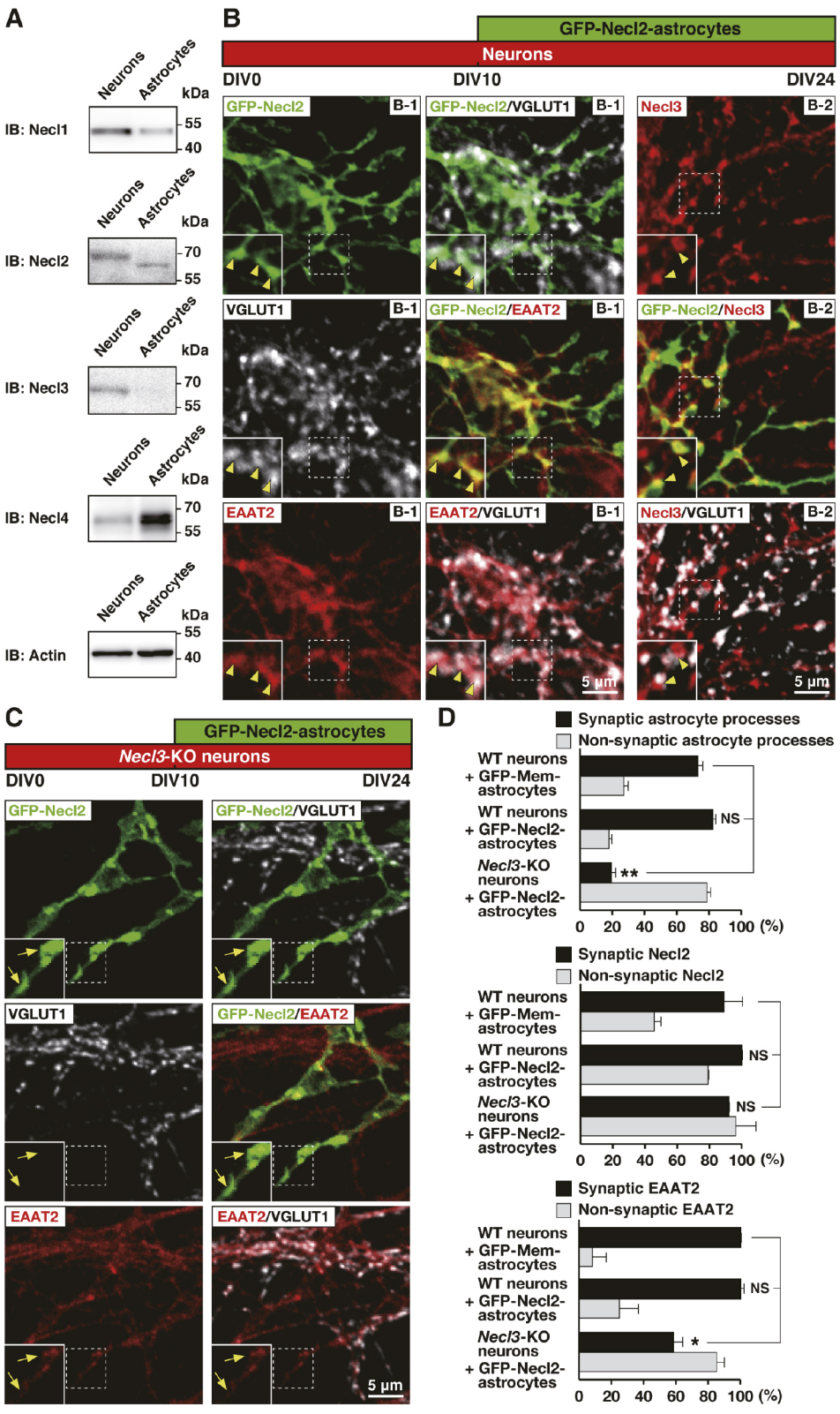

Fig. 3. Astrocytic Necl2-increased axonal Necl3-dependent localization of EAAT2 at the PAPs *in vitro*. (A) Western blot of Necl1/2/3/4 in WT neurons and astrocytes. (B,C) Representative IF images using the antibodies indicated in respective panels. WT neurons or *Necl3*-KO neurons precultured for 10 days, followed by co-culture with GFP-Necl2-astrocytes for an additional 14 days. Boxed regions are magnified in insets. (B) WT neurons and GFP-Necl2-astrocytes. Yellow arrowheads indicate the PAPs with the VGLUT1, EAAT2, Necl2 or Necl3 signal. The labels B-1 and B-2 each refer to images in the same field. (C) *Necl3*-KO neurons and GFP-Necl2-astrocytes. Yellow arrows indicate the PAPs with the EAAT2 signal and without the VGLUT1 signal. (D) Quantification of the astrocytic terminal processes that reached VGLUT1 signal-positive synapses and of the localization of the Necl2 and EAAT2 signal-positive puncta in B and C. The astrocytic terminal processes that reached VGLUT1 signal-positive synapses were defined as 'synaptic astrocyte processes' and those that did not were defined as 'non-synaptic astrocyte processes'. Data are mean±s.e.m. **P*<0.05, ***P*<0.01 (one-way ANOVA, followed by Tukey-Kramer honestly significant difference post-hoc test). NS, not significant. Images are representative of three independent experiments.

co-cultured GFP-Mem-astrocytes or GFP-Necl2-astrocytes (Fig. 3C,D; Fig. S3B-1,B-2,C; see Fig. 4D,F). The *Necl3*-KO neurons were prepared from the systemic *Necl3*-KO mice (Fig. S4C,D). Finally, genetic *Necl2* ablation in astrocytes combined with genetic *Necl3* ablation in neurons in the co-culture system resulted in a reduction of the astrocytic EAAT2 and neuronal Necl2 signals near VGLUT1 signal-positive synapses (Fig. 2B-1-B-2,C, see Fig. 4E). Essentially the same results were obtained for EAAT1 and Kir4.1 (Figs S6A-G, S7A-G; see Fig. 4). Collectively, these results indicate that astrocytic Necl2 *trans*-interacts with axonal Necl3 and recruits EAAT1/2 and Kir4.1 to the PAPs, causing astrocyte-synapse interactions and astrocyte functional polarization. It was noted that

Development (2023) 150, dev200931. doi:10.1242/dev.200931

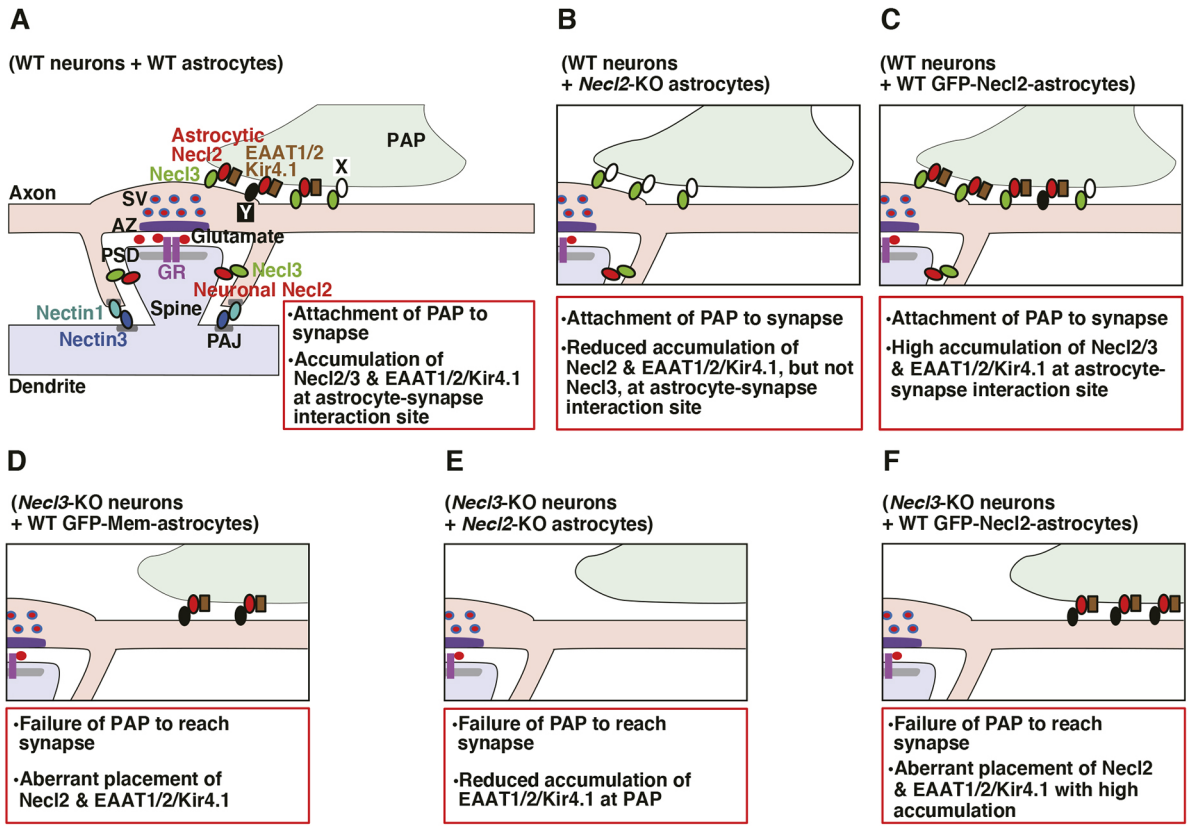

Fig. 4. Schematic of the localization of Necl2/3 and EAAT1/2/Kir4.1 at tripartite synapses in various co-culture conditions. (A-F) Differences for each combination of the co-cultures are shown in the boxes. AZ, active zone; GR, glutamate receptor; PSD, postsynaptic density; SV, synaptic vesicles.

the numbers of the Necl3 signal-positive puncta were not significantly different among conditions in which either GFP-Mem-astrocytes, GFP-Necl2-astrocytes or *Necl2*-KO GFP-Mem-astrocytes were co-cultured with WT neurons, whereas the Necl3 signal-positive puncta were not detected when either GFP-Mem-astrocytes, GFP-Necl2-astrocytes, *Necl2*-KO GFP-Mem-astrocytes were co-cultured with *Necl3*-KO neurons (Fig. S8).

Even without astrocytic Necl2, astrocytic terminal processes still extended and reached VGLUT1 signal-positive synapses but were associated with the reduced EAAT1/2 and Kir4.1 signal-positive puncta (Fig. 2A-1-A-3,C; Fig. S3A-1-A-3,C; see Fig. 4A,B). In addition, the Necl3 signal accumulation near VGLUT1 signal-positive synapses was not significantly reduced (Fig. S3A-1-A-3,C, Fig. S8). These results suggest the presence of an unidentified astrocytic X factor other than Necl2 that might *trans*-interact with axonal Necl3 for extension of astrocytic terminal processes to synapses and the axonal localization of Necl3. Conversely, even without neuronal Necl3, astrocytic terminal processes were associated with the delocalized Necl2, EAAT1/2 and Kir4.1 signal-positive puncta, although they failed to reach VGLUT1 signal-positive synapses (Fig. 2A-1-A-3; Fig. S3B-1,B-2,C; see Fig. 4A,D). These results suggest the presence of an unidentified axonal Y factor other than Necl3 that might *trans*-interact with astrocytic Necl2 for the localization of Necl2, EAAT1/2 and Kir4.1 at astrocytic terminal processes, but the unidentified axonal factor Y might be unable to extend them to reach synapses.

Furthermore, exogenous GFP-Necl2 expression in astrocytes, genetic *Necl2* ablation in astrocytes or genetic *Necl3* ablation in neurons did not affect overall astrocyte ramifications (Fig. S9), indicating that neither astrocytic Necl2 nor neuronal Necl3 is essential for the initial branching step.

In transmission electron microscopy (TEM), the elaborate terminal processes of GFP-Mem-astrocytes co-cultured with WT neurons approached synapses, but hardly enwrapped them (Fig. 5A). However, overexpression of GFP-Necl2 in astrocytes induced more extensive interactions of astrocytes with synapses to form tripartite-like glutamatergic synapses (Fig. 5B). The extrasynaptic interactions of axons with astrocytic processes were observed, and the extrasynaptic interactions of dendrites with astrocytic processes were observed to a lesser extent. The length of axons and dendrites in contact per 100 µm^2 of the PAPs of GFP-Mem-astrocytes was 13.38 µm and 5.92 µm, respectively, with the ratio of axons:dendrites being 69%:31%; whereas for GFP-Necl2 astrocytes the results were 23.08 µm and 5.66 µm, respectively, with a ratio of 80%:20% (Fig. 5A,B). Furthermore, the plasma membranes of the PAPs and presynaptic axons at their interaction sites were not thickened, compared with those at postsynaptic densities. These results indicate the preferential interactions of astrocyte fine terminal processes with axons, possibly through astrocytic Necl2 and axonal Necl3, and subsequent tripartite-like synapse formation.

Astrocytic Necl2 and axonal Necl3 promote an increase in functional synapse number *in vitro*

Astrocytes release many substances that increase synapse number and size (Nishida and Okabe, 2007; Ullian et al., 2001). Therefore, we next evaluated synaptic properties of neurons co-cultured with astrocytes using the whole-cell patch-clamp technique. Frequencies of miniature excitatory postsynaptic current (mEPSCs) were unaltered by co-culture of WT neurons with GFP-Mem-astrocytes (Fig. 6A-D). However, the co-culture of WT neurons with

Development (2023) 150, dev200931. doi:10.1242/dev.200931

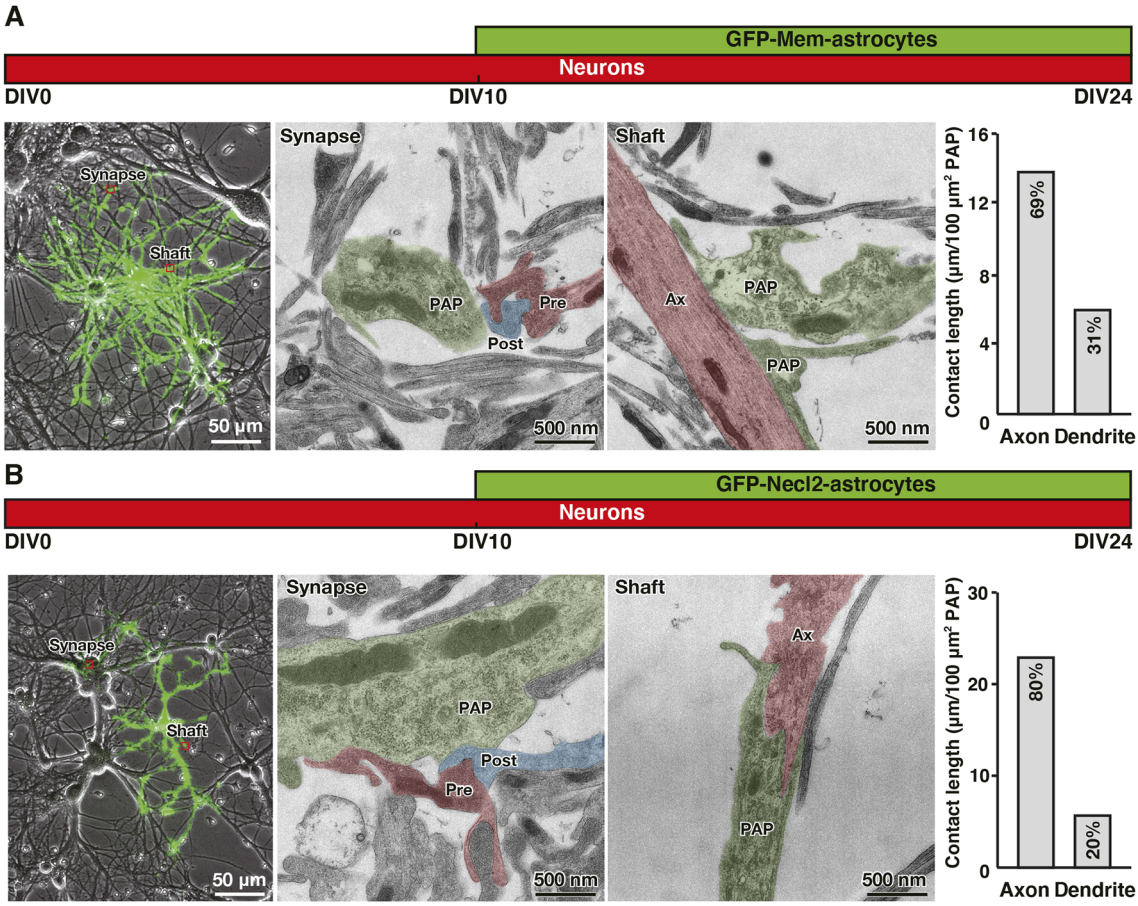

Fig. 5. Astrocytic Necl2-increased tripartite synapse formation *in vitro*. (A,B) Representative IF images using the anti-GFP monoclonal antibody and TEM. WT neurons precultured for 10 days, followed by co-culture with GFP-Mem-astrocytes (A) or GFP-Necl2-astrocytes (B) for an additional 14 days. Left images show IF images; center images show TEM images of a synapse; right images show TEM images of an axon shaft. The length of axons and dendrites in contact per 100 µm^2 of PAP are shown in the bar graphs. Ax, axon shaft; PAP, perisynaptic astrocyte process; Pre, presynapse; Post, postsynapse. Images are representative of three independent experiments.

GFP-Necl2-astrocytes increased mEPSC frequency. The increase in mEPSC frequency may reflect an increase in the number of AMPA receptor and/or glutamate release sites, but the co-culture of WT neurons with GFP-Mem- or GFP-Necl2-astrocytes did not affect mEPSC amplitude. These results suggest that the co-culture of WT neurons with GFP-Necl2-astrocytes increases sites of glutamate release from presynaptic axon terminals. To confirm this effect, we next counted the number of synapses along dendrites in neurons co-cultured with astrocytes. The co-culture of WT neurons with GFP-Mem-astrocytes increased the number of synapses with the VGLUT1 and neurabin II signals, and the co-culture of WT neurons with GFP-Necl2-astrocytes further enhanced this number (Fig. 6E,F). Collectively, these results suggest that astrocytic Necl2 at least partly increases the number of functional excitatory synapses presumably by its *trans*-interaction with axonal Necl3.

Astrocytic Necl2 and axonal Necl3 are involved in astrocyte functional polarization and tripartite synapse formation *in vivo*

In the next set of experiments, we confirmed our *in vitro* findings in the co-culture system for astrocytes and neurons by taking advantage of *in vivo* analysis using *Necl2*-KO, *Necl3*-KO and *Necl2/3* double KO (dKO) mice. First, immunolocalization of the Necl family proteins in WT mice confirmed their localizations in astrocytes and neurons. Low magnification immunofluorescence (IF) microscopy showed the robust accumulation of the Necl2/3 signals and the presence of the Necl1/4 signals at the CA3 stratum lucidum (Fig. 7A). Super-resolution structured illumination microscopy (SIM) revealed the Necl2/3 signal localization at mossy fiber synapses, which were identified by the presynaptic marker VGLUT1 and the PAJ marker Nectin3 (Fig. 7B, see Fig. 9F). The Necl2/3, VGLUT1 and Nectin3 signals partly overlapped one another and the EAAT2 signal. In immunoelectron microscopy (IEM), the Necl2 immunogold particles localized at a process-like structure of putative astrocytes facing pyramidal cell dendrites, whereas the Necl3 particles localized at mossy fiber axon terminals facing a process-like structure of putative astrocytes (Fig. 8, see Fig. 9F). In addition, the Necl2/3 particles localized at both pyramidal cell dendrites and associated mossy fibers, respectively (Fig. 8, see Fig. 9F). These analyses of Necl2/3 localization are consistent with their distributions in the co-culture system for astrocytes and neurons.

We next examined distributions of Necl2/3 and EAAT2 in multiple KO mice. IF confocal microscopy (IFCM) and SIM on *Necl2*-KO mice did not detect a reduction in the Necl3 and EAAT2 signal-positive puncta at the CA3 stratum lucidum (Fig. S10A,B), which was inconsistent with the *in vitro* co-culture results (Fig. S3A,C). The exact reason for this difference is unknown,

Development (2023) 150, dev200931. doi:10.1242/dev.200931

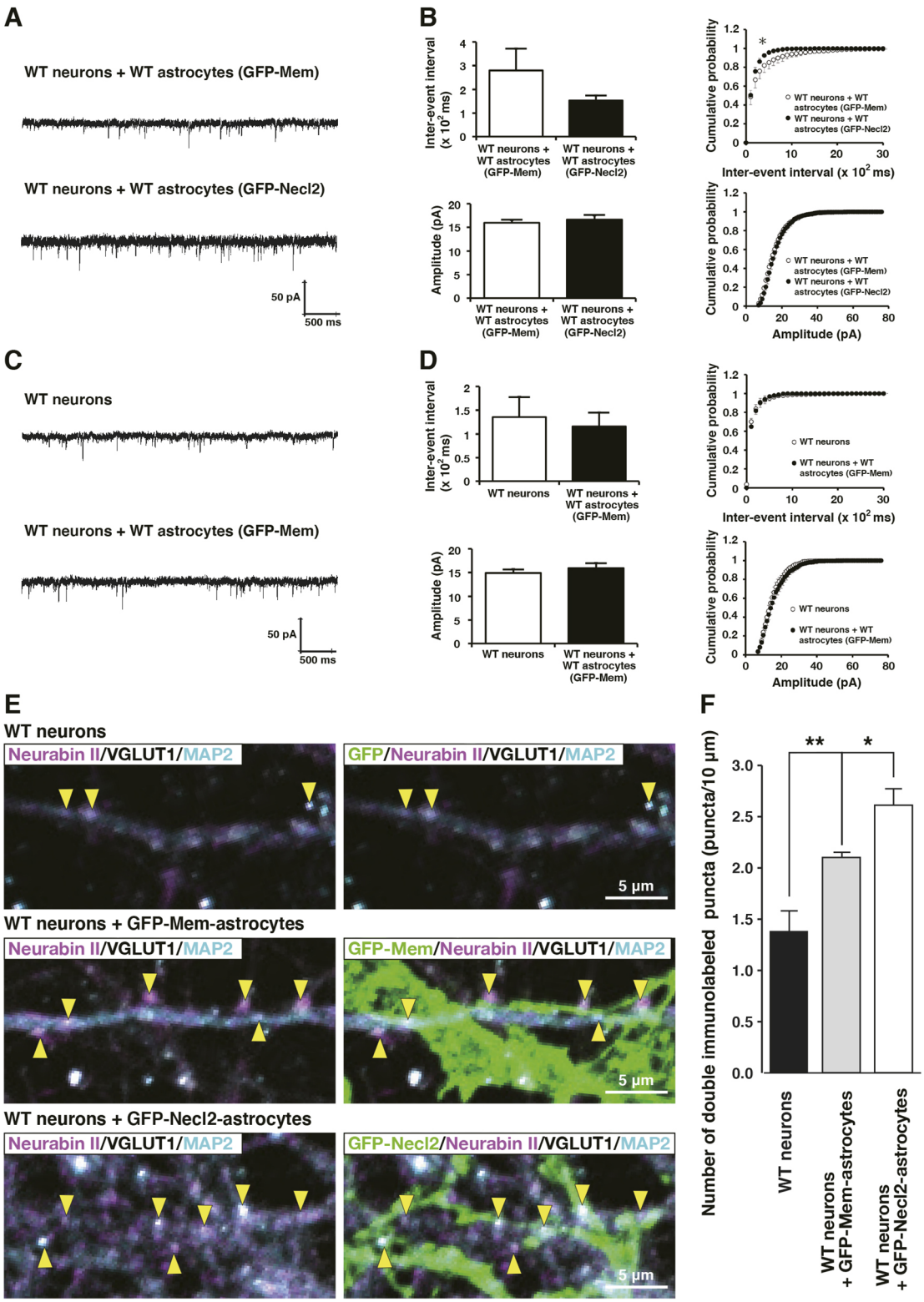

Fig. 6. Astrocytic Necl2- and axonal Necl3-increased functional synapse number *in vitro*. (A-D) Basic electrophysiological properties of synaptic transmission. WT neurons cultured alone for 24 days or precultured for 10 days, followed by co-culture with GFP-Mem- or GFP-Necl2-astrocytes for an additional 14 days. (A,C) Sample traces of mEPSCs recorded from these cultured neurons. (B,D) mEPSC inter-event intervals and amplitude. Left panel shows averaged inter-event intervals and amplitude; right panel shows cumulative probability of inter-event intervals and amplitude of mEPSCs. **P*<0.05 (Kolmogorov–Smirnov test). (E,F) Synapse number. (E) Representative IF images using antibodies indicated in respective panels. WT neurons cultured alone for 24 days or precultured for 10 days, followed by co-culture with GFP-Mem- or GFP-Necl2-astrocytes for an additional 14 days. Yellow arrowheads indicate the puncta with the VGLUT1 and neurabin II signal. (F) Number of the VGLUT1 and neurabin II double-immunolabeled puncta along a dendritic segment in E. **P*<0.05, ***P*<0.01 (one-way ANOVA, followed by Tukey-Kramer honestly significant difference post-hoc test). Data are mean±s.e.m. Images are representative of three independent experiments.

Development (2023) 150, dev200931. doi:10.1242/dev.200931

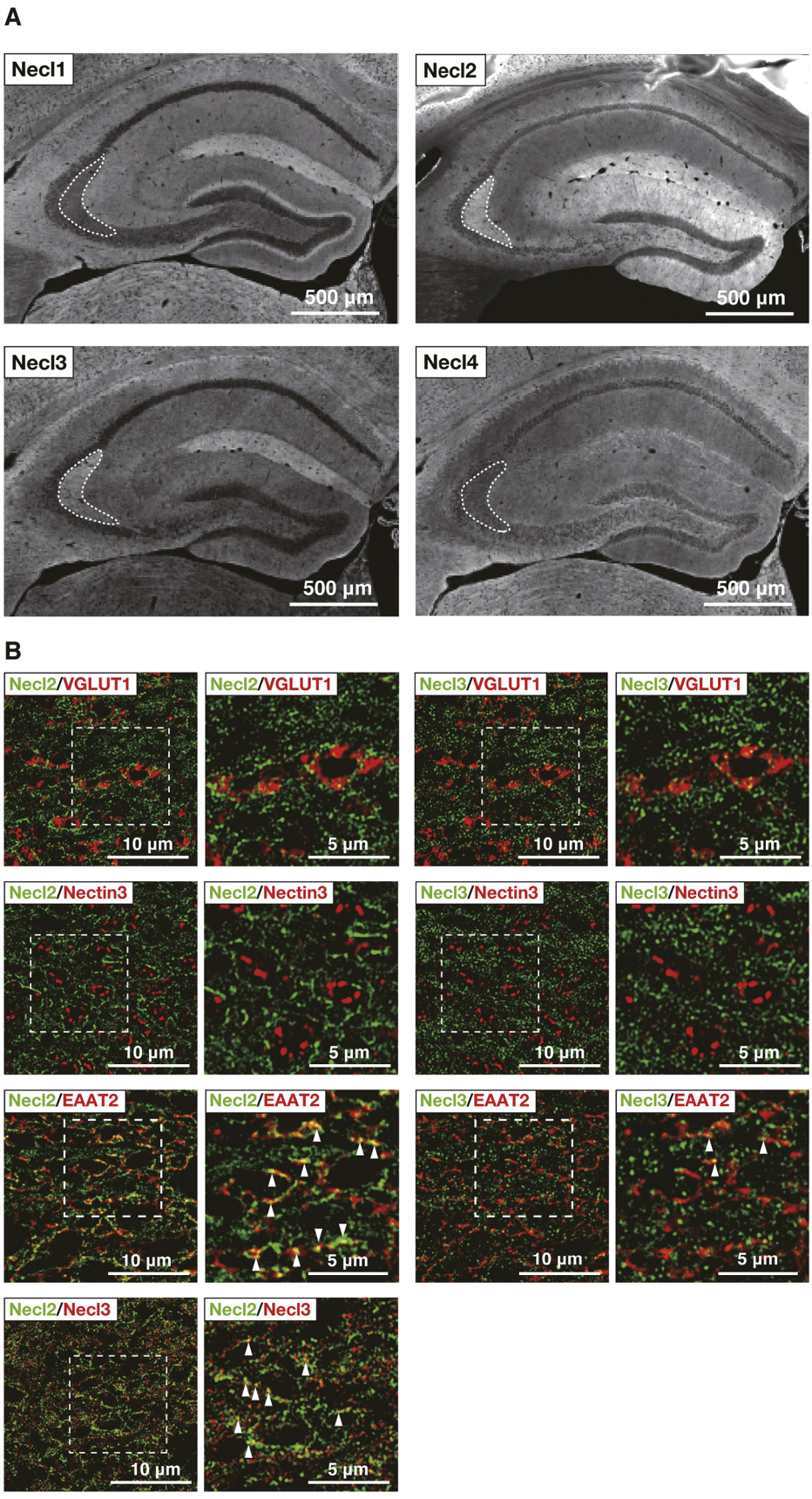

Fig. 7. Localization of Necl2/3 in the hippocampus *in vivo*. Representative IF images of hippocampi in WT mice at P56 using the antibodies indicated in respective panels. (A) Low-magnification images. Dotted lines indicate the stratum lucidum. (B) SIM images of the CA3 stratum lucidum. Arrowheads indicate colocalization of the Necl2/3 signals or the Necl2/3 and EAAT2 signals. Images are representative of three independent experiments.

Development (2023) 150, dev200931. doi:10.1242/dev.200931

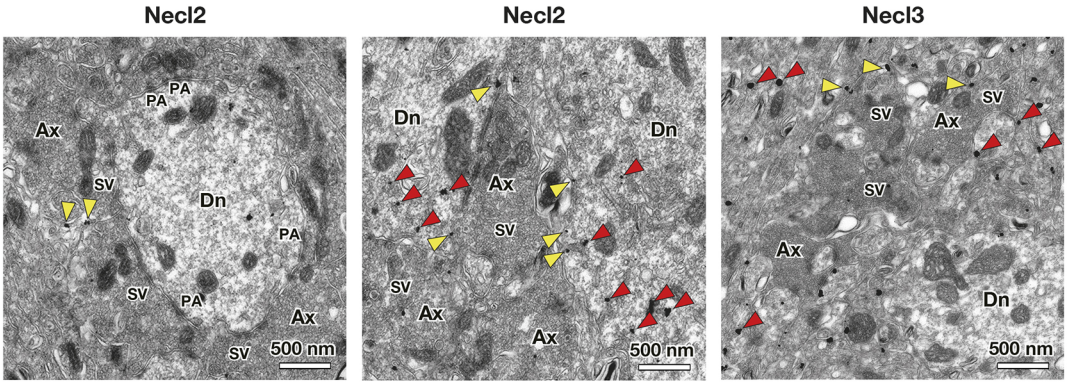

Fig. 8. Ultrastructural localization of Necl2/3 in the hippocampus *in vivo*. IEM images of Necl2/3 at mossy fiber synapses. Yellow arrowheads (left panel) indicate localization of the Necl2 immunogold particles at a process-like structure of putative astrocytes facing pyramidal cell dendrites; yellow arrowheads (center panel) indicate localization of the Necl2 particles at mossy fiber-pyramidal cell dendrite contact; red arrowheads (center panel) indicate localization of the Necl2 particles in pyramidal cell dendritic shafts; yellow arrowheads (right panel) indicate localization of the Necl3 immunogold particles at mossy fiber axon terminals facing to a process-like structure of putative astrocytes; red arrowheads (right panel) indicate localization of the Necl3 particles along the surface of small-caliber axons. Ax, axon; Dn, dendrite; PA, puncta adherentia junctions; SV, synaptic vesicle. Images are representative of three independent experiments.

but the less severe phenotype of *Necl2*-KO *in vivo* may reflect developmental compensation of Necl2 function by other molecules and/or the possible existence of an unidentified astrocytic X factor that *trans*-interacts with mossy fiber axon terminal Necl3. In *Necl3*-KO mice, IFCM detected a reduction in the Necl2 signal at the CA3 stratum lucidum (Fig. S10A). SIM on *Necl3*-KO mice revealed an expansion of EAAT2-negative spaces (Fig. S10C,D), consistent with the *in vitro* co-culture results (Fig. S3B). This SIM analysis failed to detect misplaced EAAT2 signal-positive puncta near mossy fiber synapses (Fig. S10B), which were detectable *in vitro* (Fig. S3B). This discrepancy may be due to the limited ability of SIM analysis to detect subtle changes in the position of EAAT2 signal-positive puncta in fixed brain sections having a high density of synapses. IFCM analysis on *Necl2/3*-dKO mice detected a reduction in the EAAT2 signal at the CA3 stratum lucidum (Fig. 9A-C), and detailed SIM analysis on *Necl2/3*-dKO mice revealed the fragmented and shortened EAAT2 signal, compared with that in WT mice (Fig. 9D,E). Essentially the same results were obtained for EAAT1 and Kir4.1, although a reduction in the Kir4.1 signal in *Necl2/3*-dKO mice was observed in the hippocampal CA1 region (CA1), but not in CA3 (Fig. S11A-E). The reason why the reduction in the Kir4.1 signal was not observed in CA3 was due to the technical difficulty of comparing it between WT and *Necl2/3*-dKO mice, because it was not uniformly distributed in the hippocampus, particularly in CA3; therefore, it seems prudent to reserve judgment regarding the reduction in the Kir4.1 signal in CA3. In addition, although the size of mossy fiber synapses estimated by the synapse marker bassoon did not change, the astrocyte area covering each synapse was reduced in *Necl2/3*-dKO mice, compared with those in WT mice (Fig. 9D,E; Fig. S11D,E). These *in vivo* data support the idea of Necl2/3-dependent mechanisms for astrocyte-synapse interactions as summarized in Fig. 9F, in which Necl2 localization at the PAPs, the presence of Necl3 at mossy fibers, their *trans*-interactions and subsequent functional differentiation of mossy fiber tripartite synapses are shown.

DISCUSSION

In our *in vitro* co-culture system for astrocytes and neurons, highly ramified astrocyte morphology and formation of the numerous PAPs were regulated by the presence of neurons. Astrocyte morphology in the co-culture could be classified into three types. The first type has processes extensively branched to generate numerous fine terminal processes, the second type has primary branches radiating from cell somata with few fine terminal processes, and the third type displays polygonal morphology with few primary branches (Fig. S1B). Abundance of the first and second types was sensitive to culture conditions and the two were inversely correlated, indicating possible interconversion between these two types. In contrast, the third type was present exclusively in spaces without nearby neurons and morphologically similar to astrocytes cultured without neurons. Without nearby synaptic sites releasing glutamate, this third type of astrocyte may not receive appropriate local triggers for ramifications.

During brain development, synapses are formed first, followed by astrocyte ramifications to form tripartite synapses (Farhy-Tselnicker and Allen, 2018). Synapse formation starts during the first postnatal week, peaks on postnatal day (P) 14, and is stabilized between P21 and P28. On the other hand, mouse cortical astrocytes are largely underdeveloped on P7 but rapidly develop between P7 and P26, and glutamatergic synapse signaling is involved in perisynaptic ensheathing of astrocyte processes on synapses (Morel et al., 2014). Therefore, mixing astrocytes during the synaptogenic period that occurs after days *in vitro* (DIV) 10 in the *in vitro* co-culture system for astrocytes and neurons makes sense and at least partly reflects physiological astrocyte ramifications. Our detailed *in vitro* analysis indicates that extensive astrocyte ramifications were dependent on the number and maturational levels of synapses. These synapse-dependent astrocyte ramifications were dependent on neuronal activity and were inhibited by the mGluR5 antagonist, suggesting the involvement of synaptically-released glutamate and astrocytic mGluR5 in these processes. These *in vitro* results were consistent with previous *in vivo* observations that genetic ablation of astrocytic mGluR5 or pharmacological inhibition of mGluR5 using its antagonist, MPEP, reduces astrocyte ramifications in mouse cortex (Morel et al., 2014). Furthermore, another report confirmed the mGluR5-dependent regulation of PAP remodeling by showing that synaptic activity elevates PAP movement and spine coverage via mGluR5 in the mouse hippocampus (Bernardinelli et al., 2014). Multiple lines of evidence, including our present findings, support essential roles of synaptically-released glutamate in astrocyte-synapse interactions, although alternative signaling pathways, independent of synaptic glutamate signaling, could not be completely excluded.

Development (2023) 150, dev200931. doi:10.1242/dev.200931

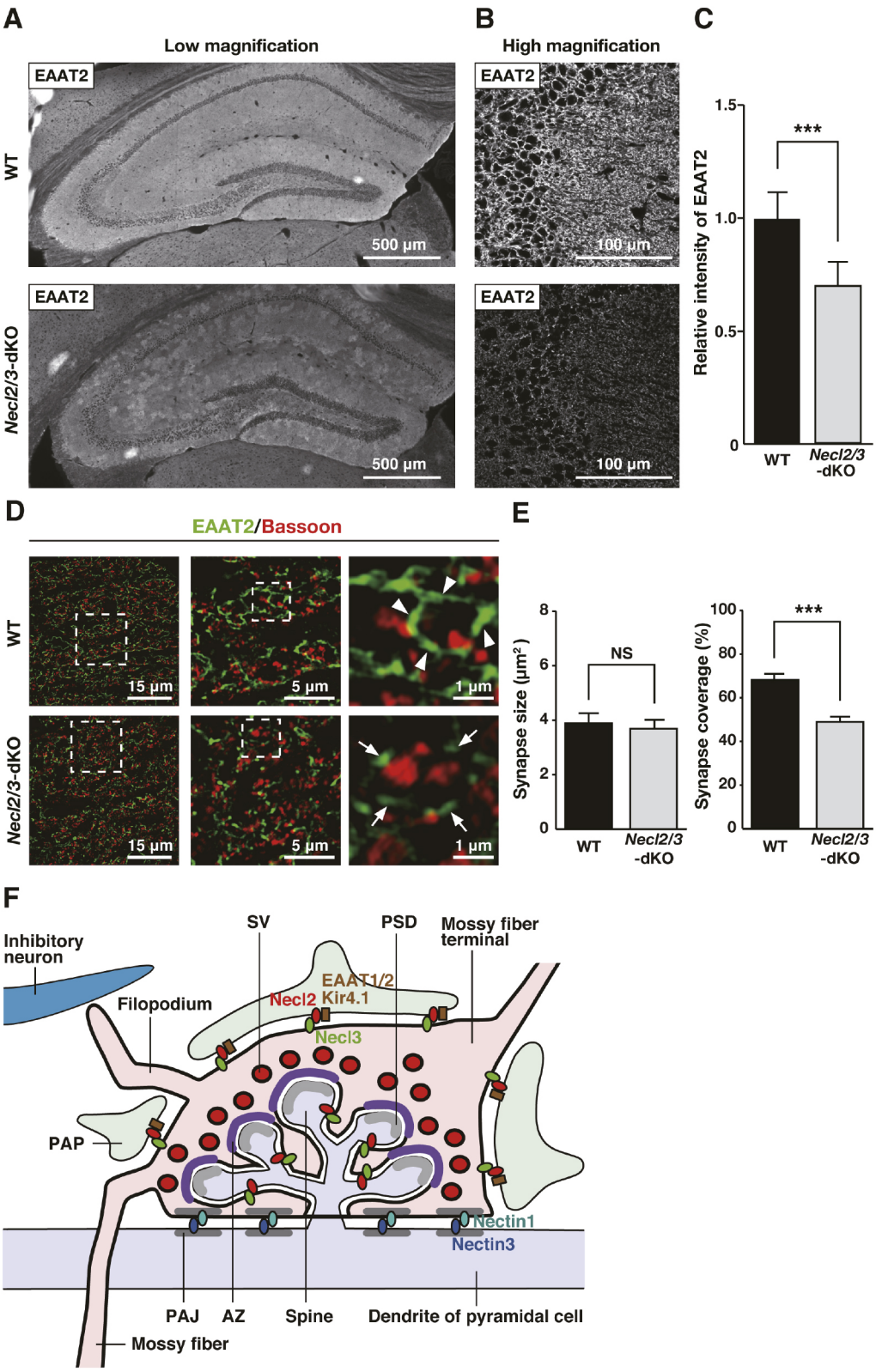

Fig. 9. Astrocytic Necl2- and axonal Necl3-dependent tripartite synapse formation and localization of EAAT2 at the PAPs in the hippocampus. (A,B) Representative IFCM images of hippocampi in WT or *Necl2/3*-dKO mice at P56 using the anti-EAAT2 polyclonal antibody. Low magnification (A) and high magnification (B) images of CA3. (C) Quantification of the mean fluorescence intensity of EAAT2 in B (n=3). ***P<0.001 (unpaired two-tailed Student's t-test). (D) SIM images of CA3. Arrowheads indicate linear pattern of the EAAT2 signal around mossy fiber axon terminal boutons; arrows indicate fragmented pattern of the EAAT2 signal around mossy fiber axon terminal boutons. (E) Quantification of the size of mossy fiber synapses in D (36 synapses were analyzed from three WT mice and 27 synapses from three *Necl2/3*-dKO mice) and the synaptic coverage ratio by astrocytes in each mossy fiber synapse in D (31 synapses were analyzed from three WT mice and 20 synapses from three *Necl2/3*-dKO mice). ***P<0.001 (unpaired two-tailed Student's t-test). NS, not significant. Images are representative of three independent experiments. (F) Schematic of the localization of Necl2/3 and EAAT2 at tripartite mossy fiber synapses. AZ, active zone; PSD, postsynaptic density; SV, synaptic vesicles. The putative unidentified astrocytic X factor that may *trans*-interact with mossy fiber axon terminal Necl3 or the putative unidentified mossy fiber axon terminal Y factor that may *trans*-interact with astrocytic Necl2 is not shown. Data are mean±s.e.m.

The highly ramified morphology of astrocytes requires direct interactions with neuronal processes (Araque et al., 1999; Haydon, 2001; Mauch et al., 2001). Astrocyte ramifications in mouse cortex are initiated in parallel with the growth and functional maturation of synapses (Freeman, 2010). However, the extent of astrocyte ramifications in early postnatal neocortex is not as high as that of the first type of astrocytes in our *in vitro* co-culture system for astrocytes and neurons. Our time-lapse imaging revealed that the initial contact of astrocytes with neuronal processes triggered the subsequent extensive ramifications. This phenomenon is similar to the so called 'contact inhibition of cell movement' (Abercrombie and Heaysman, 1954; Fisher and Yeh,

Development (2023) 150, dev200931. doi:10.1242/dev.200931

1967). When moving cells make contact with each other, they stall and then change direction to avoid further contact. Once proliferating cells reach high confluency, they become stationary and start to form cell junctions (Bell, 1978). In our co-culture system, moving astrocytes stop moving upon contact with neurites and then initiate ramifications. Once astrocytic terminal processes reach synapses, they contribute to tripartite synapse formation. For tripartite synapse formation, astrocytes first need to induce ramifications and their processes need to extend closer to synapses. Here, we showed that synaptically-released glutamate was involved in this process. On the other hand, astrocytes secrete a variety of factors that regulate synapse formation, including ApoE3, cholesterol, thrombospondin, SPARC, hevin, glypican, TGF-β and chordin-like 1 (Allen et al., 2012; Blanco-Suarez et al., 2018; Christopherson et al., 2005; Diniz et al., 2012; Jones et al., 2011; Kucukdereli et al., 2011; Perea et al., 2009; Sun et al., 1998). These factors may affect glutamate-mediated astrocyte ramifications, extension of processes to synapses and synapse-PAP interactions. Their possible involvement in astrocyte ramifications is currently under investigation, but our newly developed co-culture system might be useful for elucidating this issue.

Our *in vitro* co-culture system for astrocytes and neurons further revealed that astrocyte-synapse interactions were mediated by astrocytic Necl2 and axonal Necl3 *trans*-interaction and by additional unidentified astrocytic X and axonal Y factors. These *in vitro* observations were confirmed by *in vivo* analyses on *Necl3*-KO and *Necl2/3*-dKO mice. However, the present study did not show the evidence that the Necl2/3 *trans*-interaction is direct and therefore the possibility that this *trans*-interaction is indirect through other molecules cannot be completely excluded; however, this possibility is unlikely because the direct Necl2/3 *trans*-interaction has been previously shown (Fogel et al., 2007; Mizutani and Takai, 2016; Mizutani et al., 2021). In addition, Necl 2/3 localized at pyramidal cell dendritic spines and mossy fiber axon terminals interacting with these dendritic spines, respectively, possibly mediating mossy fiber axon terminal-dendritic spine interactions (Fig. 9F). Cell adhesions formed by the Necl2/3 *trans*-interaction in hippocampal mossy fiber tripartite synapses were structurally different from PAJs, but similar to the nectin/Necl spots (Mizutani et al., 2021). Therefore, we refer to these sites of the Necl2/3 *trans*-interaction as Necl2/3 spots.

Several astrocytic CAMs that are involved in astrocyte-synapse interactions and their modes of action have been reported. For example, γ-protocadherins promote both excitatory and inhibitory synaptogenesis in an astrocyte-neuron contact-dependent manner, and loss of astrocytic γ-protocadherins results in delayed synaptogenesis *in vivo* (Garrett and Weiner, 2009). Connexin 30 regulates astrocyte morphology and motility in a manner independent of its channel function, and loss of connexin 30 causes astrocyte invasion into synaptic clefts, resulting in an enhanced glutamate uptake (Pannasch et al., 2014). NrCAM expressed in neurons and astrocytes regulates GABAergic synapse formation and function, and loss of perisynaptic NrCAM *trans*-interaction results in significant deficits of GABAergic transmission, with a slight reduction in the amplitude of glutamatergic responses (Takano et al., 2020). In addition, it was recently shown that astrocytic neuroligin 2 regulates cortical glutamatergic synapse formation (Stogsdill et al., 2017). Collectively, these previous and present results indicate that astrocytic CAMs are involved not only in physical astrocyte-synapse interactions but also in the proper function of astrocytes to neurons. However, it remains unknown how these previously reported CAMs and Necl2/3 cooperatively, complementarily or independently regulate astrocyte-synapse interactions and astrocyte functional polarization.

Molecules essential for astrocytic functions, such as EAAT1/2 and Kir4.1, show highly polarized distributions and are enriched in the PAPs (Lehre et al., 1995; Olsen and Sontheimer, 2008). However, mechanisms for this astrocyte functional polarization remain unknown. We showed here for the first time that the Necl2/3 spots are involved in recruiting EAAT1/2 and Kir4.1 to the PAPs to induce astrocyte functional polarization. It remains unknown how the Necl2/3 spots interact with EAAT1/2 and Kir4.1, but direct or indirect *cis*-interactions may be involved. The nectin/Necl family members *cis*-interact with growth factor receptors, such as platelet-derived growth factor, fibroblast growth factor, vascular endothelial growth factor, prolactin receptors and ErbB2/3 through their extracellular regions (Mizutani and Takai, 2016). Similar mechanisms for higher-order membrane protein organization may also apply to Necl2 interactions with EAAT1/2 and Kir4.1.

The results of whole-cell patch-clamp recording and synapse counting support the idea that Necl2/3 promotes an increase in functional excitatory synapse number. This is the first demonstration that CAM-mediated astrocyte-synapse interactions facilitate formation and maturation of tripartite synapses. The effect of direct cell-cell interactions mediated by the Necl2/3 spots may cooperate with soluble factors released from astrocytes (Allen et al., 2012; Blanco-Suarez et al., 2018; Christopherson et al., 2005; Diniz et al., 2012; Jones et al., 2011; Kucukdereli et al., 2011; Perea et al., 2009; Sun et al., 1998). Mechanisms underlying the synapse number increase via the Necl2/3-mediated interaction require further analyses, but one possibility is that the adhesion of the PAPs and synapses reduces their physical distance, leading to enhanced effects of astrocyte-derived factors by increasing their local concentrations after release.

In this study, we provided evidence for the crucial roles of the Necl2/3 spots in astrocyte-synapse interactions and astrocyte functional polarization. Additional astrocytic X and axonal Y factors for ramifications of astrocytic processes and polarized molecular sorting may still exist (Fig. 4). It is unknown whether these factors are previously reported CAMs or novel molecules, but their identification will lead to better understanding of molecular mechanisms for astrocyte-synapse interactions and astrocyte functional polarization.

A co-culture system for astrocytes and neurons was previously reported, but these results were different from ours in several aspects (Stogsdill et al., 2017): (1) in their co-culture system, astrocytes did not fully ramify and formed the second type of astrocyte morphology shown in our co-culture system, whereas in our co-culture system, astrocytes fully ramified to form the first type of astrocyte morphology; (2) in their co-culture system, astrocyte ramifications induced by co-cultured neurons were not inhibited by TTX, whereas in our co-culture system, they were inhibited by TTX; (3) in their co-culture system, methanol treatment of neurons did not eliminate their ability to induce astrocyte ramifications, whereas in our co-culture system, it eliminated the ability of neurons to induce astrocyte ramifications. The exact reasons for these different results between the two co-culture systems are not known but may be caused by the following different experimental procedures and conditions: (1) in their co-culture system, both neurons and astrocytes prepared from the rat cortex were used, whereas in our co-culture system, neurons and astrocytes prepared from the mouse hippocampus and the mouse ganglionic eminence, respectively, were used; (2) in their co-culture system, the astrocytes were prepared in the serum-

Development (2023) 150, dev200931. doi:10.1242/dev.200931

containing condition and cultured in the serum-containing condition for 11 days, whereas in our co-culture system, the astrocytes were prepared in the serum-free condition and cultured in the serum-containing condition for 2 days at most; and (3) in their co-culture system, the astrocytes were co-cultured with the neurons for 2 days, whereas our co-culture system, the astrocytes were co-cultured with the neurons for 14 days. It is difficult to determine at present which of these differences in conditions is key for the discrepancy between their and our results on astrocyte morphogenesis, but careful comparison of these differences in conditions will lead to the identification of novel factors that regulate astrocyte-synapse interactions and astrocyte functional polarization.

Our newly developed *in vitro* co-culture system for astrocytes and neurons should be a highly useful model to investigate physiological functions of astrocyte-synapse interactions, astrocyte functional polarization and their underlying mechanisms. Furthermore, our co-culture system can be combined with experimental manipulations of environmental and genetic factors related to neurodegeneration, such as oxygen and glucose deprivation, application of amyloid β, and with experimental manipulations of Alzheimer's disease risk genes, including ApoE proteins, amyloid β precursor protein and presenilin. The sophisticated *in vitro* analytical system provides a new venue for understanding pathological changes in tripartite synapses related to human neurodegenerative diseases.

MATERIALS AND METHODS

Animals

C57BL/6J mice were purchased from CLEA Japan. P0 was defined as the day of birth. All animal experiments were performed in accordance with institutional guidelines and approved by the administrative panel on laboratory animal care of Kobe University. This study was approved by the president of Kobe University after being reviewed by the Kobe University Animal Care and Use Committee (approval No. 30-06-01), and animal experiments were conducted in accordance with regulations for animal experimentation of Kobe University.

Generation of *Necl2*-KO, *Necl3*-KO and *Necl2/3*-dKO mice

Necl2-KO mice were generated by gene targeting strategy. To replace the *Necl2* genomic region between the *Spe*I site in intron 1 and the *Bam*HI site in intron 3 with an *MC1 promoter-Neo-poly A* cassette, a targeting vector was constructed using a 12.7 kb *Spe*I fragment (from the *Spe*I site in intron 1 to the *Spe*I site in intron 3) and a 9.2 kb *Bam*HI fragment (from the *Bam*HI site in intron 1 to the *Bam*HI site in intron 3). The *MC1 promoter-diphtheria toxin A fragment-poly A* cassette was used for negative selection. The targeted region contained amino acids 99-199 of the Necl2 protein. The linearized targeting vector was transfected into 129/Sv RW4 embryonic stem cells (ESCs) (Genome Systems) by electroporation. ESCs harboring the targeted allele were selected for G418 resistance and then microinjected into C57BL/6 blastocysts to obtain chimeric mice. The chimeric mice were bred with BDF1 mice to generate heterozygous mice carrying the mutant allele. Mice were genotyped by PCR using DNA from tail biopsies. Primer sequences for genotyping were as follows: forward, 5′-AGATCTC-CCTTAGTTTGACTCATTTTGTG-3′; reverse, 5′-GCTCTGTAGC-ACGACGATCTGGG-3′. The PCR reaction consisted of 2 min at 98°C, followed by 40 cycles of 20 s at 98°C and 2 min at 68°C. The primer pair forward and reverse gave a 2.5 kb band for a WT allele and a 1.5 kb band for a mutant allele. $Necl2^{+/-}$ mice that were used to produce $Necl2^{-/-}$ mice had been backcrossed with C57BL/6 mice for more than ten generations.

Necl3-KO mice were generated using the CRISPR/Cas9 system as described previously, with slight modifications (Nagahama et al., 2020). Briefly, four single-guide RNAs (sgRNAs) targeting exon 1 of the *Necl3* gene were selected using CRISPRdirect (http://crispr.dbcls.jp/). Protospacer sequences of sgRNAs were as follows: 5′-CTCAGAAGAACTTCGCA-CCC-3′, 5′-CGCCCCCTCGCGGTGGCGAT-3′, 5′-GTAGCAGAAAG-CTCCTTACG-3′ and 5′-TACGCGGCACCTTTCGCCTT-3′. Cas9/gRNA ribonucleoprotein complex was delivered into fertilized C57BL/6 embryos by electroporation. Embryos were washed three times with Opti-MEM I (Thermo Fisher Scientific) supplemented with 0.1% polyvinyl alcohol (PVA) and once with 0.1% PVA-Opti MEM I containing Cas9 protein (200 ng/µl, Takara Bio) and sgRNAs (25 ng/µl each, Fasmac). Then embryos were placed in a line in the gap of an electrode pair (LF501PT1-10, BEX) filled with Cas9/gRNA containing 0.1% PVA-Opti-MEM I (total 5 µl in volume) and electroporation was performed. Voltage pulses (30 V, 3 ms) were applied seven times at intervals of 100 ms using an electroporator CUY21EDIT II (BEX). After electroporation, embryos were immediately collected from the electrode chamber and subjected to three washes with modified Whitten's medium. Electroporated embryos were transferred into oviducts of 0.5-day-post-coitum ICR recipients (Charles River Laboratories). Mice were genotyped by PCR using DNA from tail biopsies. Primer sequences for genotyping were as follows: forward, 5′-CTATCGG-GCCCCAGTTACAT-3′; reverse for the WT allele, 5′-AACAGCTGCAG-TAGCAATCTT-3′; reverse for the mutant allele, 5′-GATGACAAGAGG-TGGAAAGGGT-3′. The PCR reaction consisted of 2 min at 94°C, followed by 30 cycles of 10 s at 98°C, 15 s at 64°C and 15 s at 68°C. The size of the amplicon was 386 bp for a WT allele and 247 bp for a mutant allele.

To obtain *Necl2/3*-dKO mice, $Necl2^{+/-}$ mice were first crossed with $Necl3^{+/-}$ mice and $Necl2^{+/-}$; $Necl3^{+/-}$ mice generated were further crossed. The resulting WT and *Necl2/3*-dKO littermates were used.

Cell culture

Mouse hippocampal neurons for culture were prepared as described previously (Toyoshima et al., 2014). Cytosine arabinoside (2 µM) was added to the culture at DIV2. In the co-culture at DIV10 immediately before the addition of astrocytes separately prepared, astrocytes were less than 5%. Mouse astrocytes for culture were prepared by differentiation of neurospheres prepared from the mouse ganglionic eminence at embryonic day (E) 18.5, as described previously (Miyata et al., 2016). All cells were maintained in culture at 37°C in a humidified 5% CO_2 incubator.

In vitro co-culture system for astrocytes and neurons

Hippocampal neurons (6×10^4 cells/well) were precultured for 10 days in 24-well plates and then astrocytes (1×10^4 cells/well) were added, followed by co-culture for 14 days, unless otherwise specified. Experiments using pharmacological agents were performed as follows: 1 µM TTX (Fujifilm Wako Pure Chemical), 100 µM MCPG (Tocris Bioscience), 50 µM MPEP (Tocris Bioscience), 10 µM LY395756 (Tocris Bioscience), 20 µM CNQX (Tocris Bioscience) and 50 µM D-AP5 (Tocris Bioscience) were added to the *in vitro* co-culture of astrocytes with neurons at the indicated time points.

Astrocyte transfection

Cultured astrocytes were prepared by differentiation of neurospheres in medium mixed with Neurobasal medium and MEM at a ratio of 1:4, supplemented with 1% fetal bovine serum. A day after differentiation, astrocytes were transfected with pAcGFP1-Mem or pCMV-EGFP-Necl2 using Lipofectamine 2000 (Thermo Fisher Scientific), according to the manufacturer's protocol. The transfection efficiency of pAcGFP1-Mem into astrocytes was ∼30%.

Antibodies

Rabbit antiserum against Necl1 [1:300 for IF microscopy and 1:1000 for western blotting (WB)] and Necl3 (1:300 for IF microscopy and 1:1000 for WB) was prepared as described previously (Kakunaga et al., 2005; Shiotani et al., 2021). A rat anti-Necl2 monoclonal antibody (1C4-2) (1:300 for IF microscopy and 1:1000 for WB) was prepared as described (Shingai et al., 2003). The antibodies listed below were purchased from commercial sources; rat anti-GFP monoclonal antibody (1:300, Nacalai Tesque, 04404-84); guinea pig anti-VGLUT1 polyclonal antibody (1:1000, Merck Millipore, AB5905); rabbit anti-EAAT1 polyclonal antibody (1:300, Cell Signaling Technology, 5684); guinea pig anti-EAAT2 polyclonal antibody (1:300, Merck Millipore, AB1783); guinea pig anti-Kir4.1 polyclonal antibody (1:300, Alomone Labs, AGP-012); mouse anti-Necl4 monoclonal antibody

Development (2023) 150, dev200931. doi:10.1242/dev.200931

(1:300 for IF microscopy and 1:1000 for WB, NeuroMab, 75-247); mouse anti-actin monoclonal antibody (1:1000, Merck Millipore, MAB1501); rat anti-nectin 3 monoclonal antibody (1:300, MBL, D084-3); mouse anti-bassoon monoclonal antibody (1:300, Enzo Life Sciences, ADI-VAM-PS003); mouse anti-PSD95 monoclonal antibody (1:300, NeuroMab, 75-028); chicken anti-MAP2 polyclonal antibody (1:500, Abcam, ab5392); rabbit anti-neurabin II polyclonal antibody (1:300, Cell Signaling Technology, 14136). Primary antibodies were visualized using goat or donkey fluorochrome-conjugated secondary antibodies. The fluorochromes, Alexa Fluor 488, 555, 568 and 647 (1:400, Thermo Fisher Scientific) were used.

IF microscopy

IF microscopy of cultured cells was performed as described previously (Miyata et al., 2016). In brief, astrocytes cultured without hippocampal neurons, neurons cultured without astrocytes, and astrocytes co-cultured with neurons on coverslips were fixed in 2% paraformaldehyde (PFA)/PBS at room temperature (RT) for 15 min and 0.25% Triton X-100 in PBS at RT for 10 min. They were then incubated with a blocking buffer (10% normal goat or donkey serum, 1% bovine serum albumin (BSA), 0.25% Triton X-100 in PBS) at RT for 30 min. Samples were stained with the indicated antibodies at 4°C overnight, and then with appropriate fluorophore-conjugated secondary antibodies.

IF microscopy of frozen brain sections was performed as described previously (Toyoshima et al., 2014). Briefly, mice were deeply anesthetized and transcardially perfused at RT with 1× HBSS with Ca^{2+} and Mg^{2+} (Thermo Fisher Scientific) containing 10 mM HEPES, 1 mM sodium pyruvate, 4% sucrose, heparin and a protease inhibitor cocktail (cOmplete Mini; Roche Diagnostics), followed by perfusion with 2% PFA in the aforementioned HBSS-based buffer. After dehydration with 30% sucrose in PBS, whole brains were embedded in OCT compounds (Sakura Finetek). Cryostat sections were incubated at 62°C for 20 min in HistoVT One antigen retrieval solution (Nacalai Tesque) and then incubated with 1% BSA, 10% normal goat or donkey serum and 0.25% Triton X-100 in TBS at RT for 30 min. Sections were stained with the indicated antibodies, and then with appropriate fluorophore-conjugated secondary antibodies. Fluorescence microscopic image analyses were performed on a BZ-X710 All-in-One Fluorescence Microscope (Keyence) using a 20×/0.95 objective lens (Plan Apochromat numerical aperture objective lens; Nikon). Images captured on the BZ-X710 were analyzed using BZ-X-Analyzer software (Keyence). Confocal image analyses were performed on a C2 confocal laser-scanning microscope (Nikon) using a 40×/0.95 objective lens [Plan Apochromat numerical aperture lens (Nikon)]. Images captured on the C2 were analyzed using NIS Elements acquisition software (Nikon). Structured illumination image analyses were performed on an ELYRA PS.1 microscope (Carl Zeiss) using a 100×/1.46 objective lens (Plan Apochromat numerical aperture oil immersion objective lens, Carl Zeiss). Images were then reconstructed using Zen software (Carl Zeiss), based on the structured illumination algorithm.

Quantification of astrocytic terminal processes that reached VGLUT1 signal-positive synapses

For quantification of astrocytic terminal processes that reached VGLUT1 signal-positive synapses, multiple images of astrocytes expressing GFP-Mem or GFP-Necl2 were obtained and the number of terminal processes of those astrocytes were counted manually. Among the astrocytic terminal processes, those that reached VGLUT1 signal-positive synapses were defined as 'synaptic astrocyte processes' and those that did not were defined as 'non-synaptic astrocyte processes', and their percentages were calculated.

Quantification of Necl2, EAAT1/2 and Kir4.1 on astrocytic terminal processes

For quantification of Necl2, EAAT1/2 and Kir4.1 on each synaptic and non-synaptic astrocyte process, the numbers of those in which the signals for the indicated molecules were positive or negative were counted manually, and the percentages of each of them were calculated. In order to minimize the diffuse signal and the fusion of puncta, the contrast of each image was adjusted by setting the cutoff threshold at 10-12% of the maximum signal intensity in the linear range. Each channel was examined separately to identify and manually count immunopositive puncta without reducing the image resolution. For quantification of the Necl2 signal in GFP-Necl2-astrocytes, it was based on the GFP signal of GFP-Necl2.

TEM and IEM

For correlative light microscopy and TEM observations, cells were fixed with 4% PFA and 0.5% glutaraldehyde in PBS for 30 min. Samples were immersed in 1% osmium tetroxide, 1.5% potassium ferrocyanide in 0.1 M sodium cacodylate buffer for 1 h and stained with 1% tannic acid in 0.05 M sodium cacodylate buffer for 45 min. Samples were dehydrated in an ascending ethanol series and embedded in epoxy resin (Epon812, TAAB). After being incubated for 2 days at 60°C, ultra-thin sections of 50-60 nm were prepared in a Reichert ultramicrotome with a diamond knife and mounted on Formvar-coated copper slot grids. Samples attached to the grids were stained with 2% uranyl acetate and 0.4% lead citrate.

For IEM observations, WT mice (C57BL/6 male mice, P56) were deeply anesthetized and perfused with 4% PFA and 0.1% glutaraldehyde in 0.1 M phosphate buffer. Brains were removed, immersed in 4% PFA and 0.1% glutaraldehyde in 0.1 M phosphate buffer for 2 h. Coronal sections (50 µm) were made using a vibratome (VT-1000S, Leica). Sections were immersed in 30% sucrose in 0.1 M phosphate buffer for 1 h and then frozen with liquid nitrogen and subsequently thawed. Samples were blocked with 20% normal goat serum (NGS) in TBS for 1 h and then reacted with primary antibodies in 10% NGS in TBS at 4°C for 72 h. Samples were reacted with secondary antibodies conjugated with 1.4 nm colloidal gold [Nanogold®-IgG goat anti-rabbit IgG (H+L), Nanoprobes] in 2% NGS in TBS at 4°C overnight. Silver intensification (HQ Silver Enhancement kit, Nanoprobes) of immunogold-stained samples was performed for 7 min. Samples were treated with 1% osmium tetroxide in 0.1 M phosphate buffer for 40 min and were then stained with 2% aqueous uranyl acetate for 35 min. Samples were dehydrated with ethanol and twice more treated with propylene oxide for 10 min. Samples were embedded in resin (Durcupan, Sigma-Aldrich) and treated for 2 days at 60°C for curing. Ultra-thin sections of 50-60 nm were prepared in a Reichert ultramicrotome with a diamond knife and mounted in Formvar-coated copper slot grids. Samples attached to grids were stained with 2% uranyl acetate and 0.4% lead citrate.

TEM images were acquired at 80keV on a transmission electron microscope (JEM-1010, JEOL) with a CMOS camera (TemCam-F216, TVIPS) at ×5000 magnification for correlative light microscopy and TEM observation, and ×8000 magnification for IEM observation.

For quantification of the IEM images, 126.12 μm^2 in 13 fields of the images of astrocytes expressing GFP-Mem and 112.5 μm^2 in 17 fields of the images of astrocytes expressing GFP-Necl2 were analyzed to ensure that the area of the PAPs to be analyzed was similar. Then, the lengths of axons and dendrites interacting with the PAPs were measured. Axons and dendrites were discriminated by the presence of synaptic vesicles and actin filaments, respectively.

WB

Cells were lysed with a lysis buffer [50 mM Tris-HCl (pH 7.4), 140 mM NaCl, 1% Triton X-100, 1% sodium deoxycholate, 0.1% SDS, cOmplete Mini protease inhibitor cocktail tablets and phosphatase inhibitor cocktail 3 (Sigma-Aldrich, P0044)] on ice for 15 min. Lysates were then centrifuged at 100,000 ***g*** at 4°C for 30 min. Supernatants were subjected to SDS-PAGE and transferred to Immobilon-P polyvinylidene difluoride membranes (EMD Millipore). Membranes were blocked in 1% non-fat dry milk and then incubated with the primary antibodies, followed by incubation with HRP-conjugated secondary antibodies (1:1000, GE Healthcare Bioscience). Signals were visualized by incubation with Immobilon Western Chemiluminescent HRP Substrate (EMD Millipore, WBKLS0500) and detected using an ImageQuant LAS4000 (GE Healthcare Bioscience).

Electrophysiology

Whole-cell patch-clamp recordings from cultured hippocampal neurons were performed as described previously (Kuriu et al., 2006; Okabe et al., 1999). Cells in the culture dish were perfused with an extracellular solution [25 mM HEPES (pH 7.4), 119 mM NaCl, 2.5 mM KCl, 30 mM D-glucose,

Development (2023) 150, dev200931. doi:10.1242/dev.200931

2 mM $CaCl_2$ and 2 mM $MgCl_2$]. For measurements of mEPSCs, electrodes were filled with solution [10 mM HEPES (pH 7.4), 125 mM potassium methanesulfonate, 6 mM KCl, 2 mM $MgCl_2$, 0.6 mM EGTA, 3.2 mM Mg-ATP and 1.2 mM Na-GTP) and membrane potentials were corrected for the liquid junction potential (9 mV). mEPSCs were recorded from pyramidal neurons held at −70 mV in extracellular solution supplemented with 1 µM TTX, 1 µM strychnine (Sigma-Aldrich, S0532) and 10 µM gabazine (SR-95531) (Toronto Research Chemicals, G122500). Membrane currents were recorded using an EPC10 USB amplifier (HEKA Elektronik). Records were filtered at 1.4-2.9 kHz and acquired at 10 kHz. Series resistance was monitored during the experiments, and the cells were required to have a series resistance <20 MΩ for analysis. mEPSCs were analyzed using an Origin 8.0 pro (OriginLab), Clampfit (Molecular Devices) and Minianalysis 6.0.3 (Synaptosoft). mEPSCs were detected by setting the amplitude threshold to 6 pA (root mean square, RMS, noise level <3 pA).

Quantification of mean fluorescence intensities for the EAAT1/2 and Kir4.1 signals in the hippocampus

For quantification of mean fluorescence intensities for the EAAT1/2 and Kir4.1 signals in the hippocampus, multiple high magnification IFCM images of the WT and KO mouse pairs to be compared were obtained under the same conditions. For each image, the CA3 stratum lucidum or the area around the CA1 pyramidal cell layer was selected using the 'Freehand Selections' function of ImageJ, and the mean gray values were calculated using the 'Mean Gray Value' function. The mean gray value of the WT mice for each pair was normalized as 100%, and the percentages of the mean gray values for each pair of KO mice to be compared were calculated, then the mean of those values were calculated.

Quantification of synapse size and synapse coverage *in vivo*

For quantification of synapse size and synapse coverage *in vivo*, ∼50 cross-sectional images of mossy fiber synapses at the CA3 stratum lucidum were acquired every 0.101 µm in the *z*-axis direction. In the image at the height of the *z*-axis where the diameter of a certain synapse was the largest, the area of the synapse was calculated using the 'Freehand Selections' function of ImageJ. The length of the synaptic perimeter was also measured using the 'Freehand Selections' function, and the length of the fragmented EAAT1 or EAAT2 signal segments on the synapse perimeter was measured using the 'Freehand Line' function. Synaptic coverage was calculated by dividing the sum of the EAAT1 or EAAT2 signal segments at each synapse by the length of the synaptic perimeter.

Statistical analysis

Statistical analysis of differences between mean values was performed with two-tailed unpaired Student's *t*-tests, and the Kolmogorov–Smirnov test. For morphological analysis, one-way ANOVA was used, followed by Bonferroni correction or Tukey-Kramer honestly significant difference post-hoc test. Statistical significance was set at $P<0.05$. All values are reported as mean ±s.e.m.

Acknowledgements

We thank Aoi Ushida and Makiko Onishi for technical assistance. We thank Motoki Goto, Ryoko Kudo and Daisuke Tanaka for generation of *Necl3*-KO mice. We also thank Dr Steven D. Aird for careful editing of the manuscript.

Competing interests

O.N. is currently employed at Nissan Chemical Corporation. M.K. is currently employed at Eisai Co. All other authors declare no potential conflicts of interest.

Author contributions

Conceptualization: Y.T.; Methodology: O.N., M.M., T. Kameyama, T. Kuriu, A.A., S.O., K.M., Y.T.; Validation: O.N., M.M., H.S., T. Kameyama, R.K., T.S., T. Kuriu, Y.K., Y.S., M.K., A.A., S.O., K.M., Y.T.; Formal analysis: O.N., M.M., H.S., T. Kameyama, R.K., T.S., T. Kuriu, Y.K., Y.S., M.K., A.A., S.O., K.M., Y.T.; Investigation: O.N., M.M., H.S., T. Kameyama, R.K., T.S., T. Kuriu, Y.K., Y.S., M.K., A.A.; Writing - original draft: Y.T.; Writing - review & editing: O.N., M.M., H.S., T. Kameyama, R.K., T.S., T. Kuriu, Y.K., Y.S., M.K., A.A., S.O., K.M., Y.T.; Visualization: O.N., M.M., H.S., T. Kameyama, R.K., T.S., T. Kuriu, Y.K., Y.S., M.K., A.A., S.O., K.M.; Supervision: Y.T.; Funding acquisition: M.M., S.O., K.M.

Funding

This study was supported by Japan Society for the Promotion of Science (JSPS) Grant-in-Aid for Scientific Research (A and C) grants JP18K06513 and JP21K06410 to M.M. and JP20H00481 to S.O., by JSPS Grant-in-Aid for Transformative Research Areas grant JP20H05895 to M.M. and S.O., by Japan Agency for Medical Research and Development grants JP21gm5010001 to K.M. and JP20gm1310003 to S.O., and by Japan Science and Technology Agency Moonshot Research and Development Program grant JPMJMS2024 to K.M.

Data availability

All relevant data can be found within the article and its supplementary information.

References

Abercrombie, M. and Heaysman, J. E. M. (1954). Observations on the social behaviour of cells in tissue culture. *Exp. Cell Res.* **6**, 293-306. doi:10.1016/0014-4827(54)90176-7

Allen, P. B., Ouimet, C. C. and Greengard, P. (1997). Spinophilin, a novel protein phosphatase 1 binding protein localized to dendritic spines. *Proc. Natl. Acad. Sci. USA* **94**, 9956-9961. doi:10.1073/pnas.94.18.9956

Allen, N. J., Bennett, M. L., Foo, L. C., Wang, G. X., Chakraborty, C., Smith, S. J. and Barres, B. A. (2012). Astrocyte glypicans 4 and 6 promote formation of excitatory synapses via GluA1 AMPA receptors. *Nature* **486**, 410-414. doi:10.1038/nature11059

Araque, A., Parpura, V., Sanzgiri, R. P. and Haydon, P. G. (1999). Tripartite synapses: glia, the unacknowledged partner. *Trends Neurosci.* **22**, 208-215. doi:10.1016/S0166-2236(98)01349-6

Bambrick, L. L., de Grip, A., Seenivasan, V., Krueger, B. K. and Yarowsky, P. J. (1996). Expression of glial antigens in mouse astrocytes: species differences and regulation in vitro. *J. Neurosci. Res.* **46**, 305-315. doi:10.1002/(SICI)1097-4547(19961101)46:3<305::AID-JNR3>3.0.CO;2-O

Bell, P. B. (1978). Contact inhibition of movement in transformed and nontransformed cells. *Birth Defects Orig. Artic. Ser.* **14**, 177-194.

Bernardinelli, Y., Muller, D. and Nikonenko, I. (2014). Astrocyte-synapse structural plasticity. *Neural Plast.* **2014**, 232105. doi:10.1155/2014/232105

Blanco-Suárez, E., Caldwell, A. L. M. and Allen, N. J. (2017). Role of astrocyte-synapse interactions in CNS disorders. *J. Physiol.* **595**, 1903-1916. doi:10.1113/JP270988

Blanco-Suarez, E., Liu, T.-F., Kopelevich, A. and Allen, N. J. (2018). Astrocyte-secreted chordin-like 1 drives synapse maturation and limits plasticity by increasing synaptic GluA2 AMPA receptors. *Neuron* **100**, 1116-1132.e13. doi:10.1016/j.neuron.2018.09.043

Bonaguidi, M. A., McGuire, T., Hu, M., Kan, L., Samanta, J. and Kessler, J. A. (2005). LIF and BMP signaling generate separate and discrete types of GFAP-expressing cells. *Development* **132**, 5503-5514. doi:10.1242/dev.02166

Booher, J. and Sensenbrenner, M. (1972). Growth and cultivation of dissociated neurons and glial cells from embryonic chick, rat and human brain in flask cultures. *Neurobiology* **2**, 97-105.

Cho, K.-O., Hunt, C. A. and Kennedy, M. B. (1992). The rat brain postsynaptic density fraction contains a homolog of the drosophila discs-large tumor suppressor protein. *Neuron* **9**, 929-942. doi:10.1016/0896-6273(92)90245-9

Chojnacki, A. and Weiss, S. (2008). Production of neurons, astrocytes and oligodendrocytes from mammalian CNS stem cells. *Nat. Protoc.* **3**, 935-940. doi:10.1038/nprot.2008.55

Christopherson, K. S., Ullian, E. M., Stokes, C. C. A., Mullowney, C. E., Hell, J. W., Agah, A., Lawler, J., Mosher, D. F., Bornstein, P. and Barres, B. A. (2005). Thrombospondins are astrocyte-secreted proteins that promote CNS synaptogenesis. *Cell* **120**, 421-433. doi:10.1016/j.cell.2004.12.020

Danbolt, N. C. (2001). Glutamate uptake. *Prog. Neurobiol.* **65**, 1-105. doi:10.1016/S0301-0082(00)00067-8

Danbolt, N. C., Storm-Mathisen, J. and Kanner, B. I. (1992). An [Na++K+]coupled l-glutamate transporter purified from rat brain is located in glial cell processes. *Neuroscience* **51**, 295-310. doi:10.1016/0306-4522(92)90316-T

Danbolt, N. C., Furness, D. N. and Zhou, Y. (2016). Neuronal vs glial glutamate uptake: Resolving the conundrum. *Neurochem. Int.* **98**, 29-45. doi:10.1016/j.neuint.2016.05.009

Diniz, L. P., Almeida, J. C., Tortelli, V., Lopes, C. V., Setti-Perdigão, P., Stipursky, J., Kahn, S. A., Romão, L. F., de Miranda, J., Alves-Leon, S. V. et al. (2012). Astrocyte-induced synaptogenesis is mediated by transforming growth factor β signaling through modulation of d-serine levels in cerebral cortex neurons. *J. Biol. Chem.* **287**, 41432-41445. doi:10.1074/jbc.M112.380824

Djukic, B., Casper, K. B., Philpot, B. D., Chin, L.-S. and McCarthy, K. D. (2007). Conditional knock-out of Kir4.1 leads to glial membrane depolarization, inhibition of potassium and glutamate uptake, and enhanced short-term synaptic potentiation. *J. Neurosci.* **27**, 11354-11365. doi:10.1523/JNEUROSCI.0723-07.2007

Farhy-Tselnicker, I. and Allen, N. J. (2018). Astrocytes, neurons, synapses: a tripartite view on cortical circuit development. *Neural Dev.* **13**, 7. doi:10.1186/s13064-018-0104-y

Fisher, H. W. and Yeh, J. (1967). Contact inhibition in colony formation. *Science* **155**, 581-582. doi:10.1126/science.155.3762.581

Fogel, A. I., Akins, M. R., Krupp, A. J., Stagi, M., Stein, V. and Biederer, T. (2007). SynCAMs organize synapses through heterophilic adhesion. *J. Neurosci.* **27**, 12516-12530. doi:10.1523/JNEUROSCI.2739-07.2007

Freeman, M. R. (2010). Specification and morphogenesis of astrocytes. *Science* **330**, 774-778. doi:10.1126/science.1190928

Garrett, A. M. and Weiner, J. A. (2009). Control of CNS synapse development by γ-protocadherin-mediated astrocyte-neuron contact. *J. Neurosci.* **29**, 11723-11731. doi:10.1523/JNEUROSCI.2818-09.2009

Haydon, P. G. (2001). GLIA: listening and talking to the synapse. *Nat. Rev. Neurosci.* **2**, 185-193. doi:10.1038/35058528

Jones, E. V., Bernardinelli, Y., Tse, Y. C., Chierzi, S., Wong, T. P. and Murai, K. K. (2011). Astrocytes control glutamate receptor levels at developing synapses through SPARC-β-integrin interactions. *J. Neurosci.* **31**, 4154-4165. doi:10.1523/JNEUROSCI.4757-10.2011

Kakunaga, S., Ikeda, W., Itoh, S., Deguchi-Tawarada, M., Ohtsuka, T., Mizoguchi, A. and Takai, Y. (2005). Nectin-like molecule-1/TSLL1/SynCAM3: a neural tissue-specific immunoglobulin-like cell-cell adhesion molecule localizing at non-junctional contact sites of presynaptic nerve terminals, axons and glia cell processes. *J. Cell Sci.* **118**, 1267-1277. doi:10.1242/jcs.01656

Kucukdereli, H., Allen, N. J., Lee, A. T., Feng, A., Ozlu, M. I., Conatser, L. M., Chakraborty, C., Workman, G., Weaver, M., Sage, E. H. et al. (2011). Control of excitatory CNS synaptogenesis by astrocyte-secreted proteins Hevin and SPARC. *Proc. Natl. Acad. Sci. USA* **108**, E440-E449. doi:10.1073/pnas.1104977108

Kuriu, T., Inoue, A., Bito, H., Sobue, K. and Okabe, S. (2006). Differential control of postsynaptic density scaffolds via actin-dependent and -independent mechanisms. *J. Neurosci.* **26**, 7693-7706. doi:10.1523/JNEUROSCI.0522-06.2006

Lehre, K. P., Levy, L. M., Ottersen, O. P., Storm-Mathisen, J. and Danbolt, N. C. (1995). Differential expression of two glial glutamate transporters in the rat brain: Quantitative and immunocytochemical observations. *J. Neurosci.* **15**, 1835-1853. doi:10.1523/JNEUROSCI.15-03-01835.1995

Li, Y., Serwanski, D. R., Miralles, C. P., Fiondella, C. G., Loturco, J. J., Rubio, M. E. and De Blas, A. L. (2010). Synaptic and nonsynaptic localization of protocadherin-γC5 in the rat brain. *J. Comp. Neurol.* **518**, 3439-3463. doi:10.1002/cne.22390

Mauch, D. H., Nägler, K., Schumacher, S., Göritz, C., Müller, E.-C., Otto, A. and Pfrieger, F. W. (2001). CNS synaptogenesis promoted by glia-derived cholesterol. *Science* **294**, 1354-1357. doi:10.1126/science.294.5545.1354

Miyata, M., Mandai, K., Maruo, T., Sato, J., Shiotani, H., Kaito, A., Itoh, Y., Wang, S., Fujiwara, T., Mizoguchi, A. et al. (2016). Localization of nectin-2δ at perivascular astrocytic endfoot processes and degeneration of astrocytes and neurons in nectin-2 knockout mouse brain. *Brain Res.* **1649**, 90-101. doi:10.1016/j.brainres.2016.08.023

Mizoguchi, A., Nakanishi, H., Kimura, K., Matsubara, K., Ozaki-Kuroda, K., Katata, T., Honda, T., Kiyohara, Y., Heo, K., Higashi, M. et al. (2002). Nectin: an adhesion molecule involved in formation of synapses. *J. Cell Biol.* **156**, 555-565. doi:10.1083/jcb.200103113

Mizutani, K. and Takai, Y. (2016). Nectin spot: a novel type of nectin-mediated cell adhesion apparatus. *Biochem. J.* **473**, 2691-2715. doi:10.1042/BCJ20160235

Mizutani, K., Miyata, M., Shiotani, H., Kameyama, T. and Takai, Y. (2021). Nectins and Nectin-like molecules in synapse formation and involvement in neurological diseases. *Mol. Cell. Neurosci.* **115**, 103653. doi:10.1016/j.mcn.2021.103653

Morel, L., Higashimori, H., Tolman, M. and Yang, Y. (2014). VGluT1+ Neuronal Glutamatergic signaling regulates postnatal developmental maturation of cortical protoplasmic astroglia. *J. Neurosci.* **34**, 10950-10962. doi:10.1523/JNEUROSCI.1167-14.2014

Moriyoshi, K., Richards, L. J., Akazawa, C., O'Leary, D. D. M. and Nakanishi, S. (1996). Labeling neural cells using adenoviral gene transfer of membrane-targeted GFP. *Neuron* **16**, 255-260. doi:10.1016/S0896-6273(00)80044-6

Nagahama, K., Sakoori, K., Watanabe, T., Kishi, Y., Kawaji, K., Koebis, M., Nakao, K., Gotoh, Y., Aiba, A., Uesaka, N. et al. (2020). Setd1a insufficiency in mice attenuates excitatory synaptic function and recapitulates schizophrenia-related behavioral abnormalities. *Cell Rep.* **32**, 108126. doi:10.1016/j.celrep.2020.108126

Nagelhus, E. A., Mathiisen, T. M. and Ottersen, O. P. (2004). Aquaporin-4 in the central nervous system: cellular and subcellular distribution and coexpression with KIR4.1. *Neuroscience* **129**, 905-913. doi:10.1016/j.neuroscience.2004.08.053

Nakanishi, H., Obaishi, H., Satoh, A., Wada, M., Mandai, K., Satoh, K., Nishioka, H., Matsuura, Y., Mizoguchi, A. and Takai, Y. (1997). Neurabin: A novel neural tissue-specific actin filament-binding protein involved in neurite formation. *J. Cell Biol.* **139**, 951-961. doi:10.1083/jcb.139.4.951

Nishida, H. and Okabe, S. (2007). Direct astrocytic contacts regulate local maturation of dendritic spines. *J. Neurosci.* **27**, 331-340. doi:10.1523/JNEUROSCI.4466-06.2007

Nwaobi, S. E., Lin, E., Peramsetty, S. R. and Olsen, M. L. (2014). DNA methylation functions as a critical regulator of Kir4.1 expression during CNS development. *Glia* **62**, 411-427. doi:10.1002/glia.22613

Nwaobi, S. E., Cuddapah, V. A., Patterson, K. C., Randolph, A. C. and Olsen, M. L. (2016). The role of glial-specific Kir4.1 in normal and pathological states of the CNS. *Acta Neuropathol.* **132**, 1-21. doi:10.1007/s00401-016-1553-1

Okabe, S., Kim, H.-D., Miwa, A., Kuriu, T. and Okado, H. (1999). Continual remodeling of postsynaptic density and its regulation by synaptic activity. *Nat. Neurosci.* **2**, 804-811. doi:10.1038/12175

Olsen, M. L. and Sontheimer, H. (2008). Functional implications for Kir4.1 channels in glial biology: from K+ buffering to cell differentiation. *J. Neurochem.* **107**, 589-601. doi:10.1111/j.1471-4159.2008.05615.x

Pannasch, U., Freche, D., Dallérac, G., Ghézali, G., Escartin, C., Ezan, P., Cohen-Salmon, M., Benchenane, K., Abudara, V., Dufour, A. et al. (2014). Connexin 30 sets synaptic strength by controlling astroglial synapse invasion. *Nat. Neurosci.* **17**, 549-558. doi:10.1038/nn.3662

Perea, G., Navarrete, M. and Araque, A. (2009). Tripartite synapses: astrocytes process and control synaptic information. *Trends Neurosci.* **32**, 421-431. doi:10.1016/j.tins.2009.05.001

Reilly, J. F., Maher, P. A. and Kumari, V. G. (1998). Regulation of astrocyte GFAP expression by TGF-β1 and FGF-2. *Glia* **22**, 202-210. doi:10.1002/(SICI)1098-1136(199802)22:2<202::AID-GLIA11>3.0.CO;2-1

Satoh, A., Nakanishi, H., Obaishi, H., Wada, M., Takahashi, K., Satoh, K., Hirao, K., Nishioka, H., Hata, Y., Mizoguchi, A. et al. (1998). Neurabin-II/spinophilin: An actin filament-binding protein with one PDZ domain localized at cadherin-based cell-cell adhesion sites. *J. Biol. Chem.* **273**, 3470-3475. doi:10.1074/jbc.273.6.3470

Shingai, T., Ikeda, W., Kakunaga, S., Morimoto, K., Takekuni, K., Itoh, S., Satoh, K., Takeuchi, M., Imai, T., Monden, M. et al. (2003). Implications of Nectin-like Molecule-2/IGSF4/RA175/SgIGSF/TSLC1/SynCAM1 in Cell-Cell Adhesion and Transmembrane Protein Localization in Epithelial Cells. *J. Biol. Chem.* **278**, 35421-35427. doi:10.1074/jbc.M305387200

Shiotani, H., Miyata, M., Kameyama, T., Mandai, K., Yamasaki, M., Watanabe, M., Mizutani, K. and Takai, Y. (2021). Nectin-2α is localized at cholinergic neuron dendrites and regulates synapse formation in the medial habenula. *J. Comp. Neurol.* **529**, 450-477. doi:10.1002/cne.24958

Stogsdill, J. A., Ramirez, J., Liu, D., Kim, Y. H., Baldwin, K. T., Enustun, E., Ejikeme, T., Ji, R.-R. and Eroglu, C. (2017). Astrocytic neuroligins control astrocyte morphogenesis and synaptogenesis. *Nature* **551**, 192-197. doi:10.1038/nature24638

Sun, Y., Wu, S., Bu, G., Onifade, M. K., Patel, S. N., LaDu, M. J., Fagan, A. M. and Holtzman, D. M. (1998). Glial fibrillary acidic protein-apolipoprotein E (apoE) transgenic mice: astrocyte-specific expression and differing biological effects of astrocyte-secreted apoE3 and apoE4 lipoproteins. *J. Neurosci.* **18**, 3261-3272. doi:10.1523/JNEUROSCI.18-09-03261.1998

Takai, Y., Ikeda, W., Ogita, H. and Rikitake, Y. (2008a). The immunoglobulin-like cell adhesion molecule nectin and its associated protein afadin. *Annu. Rev. Cell Dev. Biol.* **24**, 309-342. doi:10.1146/annurev.cellbio.24.110707.175339

Takai, Y., Miyoshi, J., Ikeda, W. and Ogita, H. (2008b). Nectins and nectin-like molecules: roles in contact inhibition of cell movement and proliferation. *Nat. Rev. Mol. Cell Biol.* **9**, 603-615. doi:10.1038/nrm2457

Takano, T., Wallace, J. T., Baldwin, K. T., Purkey, A. M., Uezu, A., Courtland, J. L., Soderblom, E. J., Shimogori, T., Maness, P. F., Eroglu, C. et al. (2020). Chemico-genetic discovery of astrocytic control of inhibition in vivo. *Nature* **588**, 296-302. doi:10.1038/s41586-020-2926-0

Takeuchi, T., Duszkiewicz, A. J. and Morris, R. G. M. (2014). The synaptic plasticity and memory hypothesis: encoding, storage and persistence. *Philos. Trans. R. Soc. Lond. B. Biol. Sci.* **369**, 20130288. doi:10.1098/rstb.2013.0288

Toyoshima, D., Mandai, K., Maruo, T., Supriyanto, I., Togashi, H., Inoue, T., Mori, M. and Takai, Y. (2014). Afadin regulates puncta adherentia junction formation and presynaptic differentiation in hippocampal neurons. *PLoS ONE* **9**, 1-8. doi:10.1371/journal.pone.0089763

Ullian, E. M., Sapperstein, S. K., Christopherson, K. S. and Barres, B. A. (2001). Control of synapse number by glia. *Science* **291**, 657-661. doi:10.1126/science.291.5504.657